Supporting Information

Persistent Dimer Emission in Thermally Activated Delayed Fluorescence Materials

Marc K. Etherington*[a], Nadzeya A. Kukhta[b], Heather F. Higginbotham[a], Andrew Danos[a], Aisha N. Bismillah[b], David R. Graves[a], Paul R. McGonigal[b], Nils Haase[c,d], Antonia Morherr[c], Andrei S. Batsanov[b], Christof Pflumm[c], Vandana Bhalla[b,e], Martin R. Bryce[b], Andrew P. Monkman[a].

*E-mail: marc.k.etherington@durham.ac.uk

[a]Department of Physics and [b]Department of Chemistry, Durham University, South Road, Durham, DH1 3LE, UK

[c]Merck KGaA, Performance Materials – Display Solutions, Frankfurter Straße 250, 64293 Darmstadt, Germany

[d]Institute of Physics, Experimental Physics IV, University of Augsburg, Universitätsstr. 1, 86135 Augsburg, Germany

[e]Department of Chemistry, Guru Nanak Dev University, Grand Trunk Road, Off NH 1, Amritsar, Punjab-143005 India

Table of Contents

1. General methods

Materials: All reagents were purchased from commercial suppliers (Sigma-Aldrich, Acros, or Alfa Aesar) and used without further purification unless otherwise stated. **3-Bromocarbazole**,[1] **4CzTPN**,[2] **4CzIPN-^{t}Bu$_8$**[2] and **3,6-Di^{t}BuCz**[3] were prepared according to reported procedures.

Instrumentationa and Analytical Techniques: Analytical thin-layer chromatography (TLC) was performed on neutral aluminum sheet silica gel plates and visualized under UV irradiation (254 nm). Nuclear magnetic resonance (NMR) spectra were recorded using Bruker Advance (III)-400 (^{1}H 400.130 MHz and ^{13}C 100.613 MHz), Varian Inova-500 (^{1}H 500.130 MHz and ^{13}C 125.758 MHz), Varian VNMRS-600 (^{1}H 600.130 MHz and ^{13}C 150.903 MHz) or a Varian VNMRS-700 (^{1}H 700.130 MHz and ^{13}C 176.048 MHz) spectrometers, at a constant temperature of 298 K unless otherwise stated. For variable temperature measurements, operating temperatures were calibrated using an internal calibration solution of MeOH and glycerol. Chemical shifts (δ) are reported in parts per million (ppm) relative to the signals corresponding to residual non-deuterated solvents [$CDCl_3$: δ = 7.26 or 77.16]. Coupling constants (J) are reported in Hertz (Hz). ^{13}C NMR Experiments were proton decoupled. Assignment of ^{1}H and ^{13}C NMR signals were accomplished by two-dimensional NMR spectroscopy (COSY, NOESY, HSQC, HMBC). NMR spectra were processed using MestReNova version 11.0.0-17609. Data are reported as follows: chemical shift; multiplicity; coupling constants; integration and assignment. Low-resolution ASAP-MS and MALDI-TOF were performed using a Waters Xevo QTOF equipped with an Atmospheric Solids Analysis Probe (ASAP) and a DCTB Matrix- Assisted Laser Desorption/ionisation (MALDI) equipped with a 337 nm nitrogen laser with a reflection mode of analysis. High-resolution ASAP (HR-ASAP) mass spectra were measured using a Waters LCT Premier XE high resolution, accurate mass UPLC ES MS (also with ASAP ion source). Melting points were recorded using a Gallenkamp (Sanyo) apparatus and are uncorrected. X-Ray powder diffraction was measured on a Bruker AXS D8 Advance diffractometer with a Lynxeye Soller PSD Detector (Bragg–Brentano geometry, variable slits set at 6 mm) using Ni-filtered sealed-tube Cu-$K\alpha$ radiation (α_1/α_2 mixture with the average λ=1.5406

Å); 2θ range 30 to 100° was scanned in 0.02° steps, scan time 57 min. Differential scanning calorimetry (DSC) was peformed using a Perkin Elmer DSC 8500 running nitrogen purge gas at 30 ml per minute, with samples encapsulated in standard aluminium pans. Thermogravimetric Analysis (TGA) was performed using a Perkin Elmer TGA 8000, running in a nitrogen gas environment 30 mL per minute using ceramic pans.

2. Synthetic methods

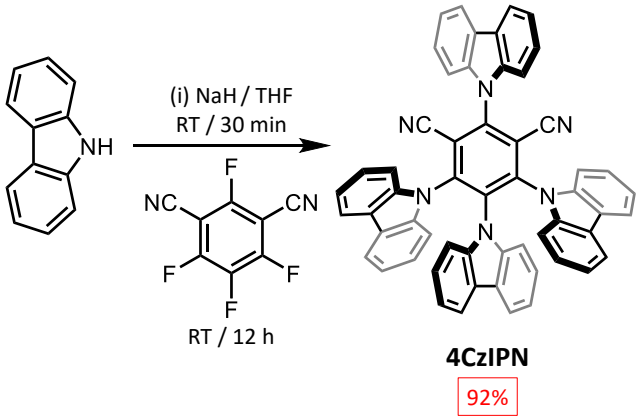

Scheme S1 The synthetic route used to prepare **4CzIPN.**

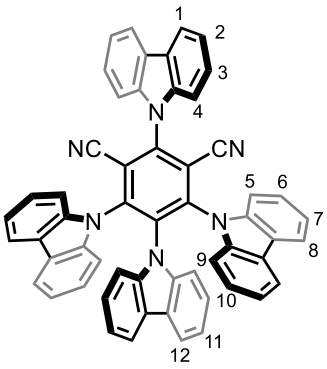

4CzIPN: Sodium hydride (0.36 g, 15 mmol) was added slowly to a stirred solution of carbazole (1.67 g, 10 mmol) in anhydrous THF (40 mL) under argon at RT. After 30 min, tetrafluoroisophthalonitrile (0.40 g, 2 mmol) was added. After stirring at RT for 12 h, 2 mL H_2O was added to the reaction mixture to quench the excess of sodium hydride. The resulting mixture was concentrated under reduced pressure and washed by H_2O and EtOH to yield the crude product. Recrystallization from chloroform/hexanes (1/4 v/v) mixture gave the title compoundas yellow crystals (1.15 g, 1.46 mmol, 92%). **M.P.** >350 °C. **^{1}H NMR** (600 MHz, DMSO-d_6) δ 8.33 (dt, 2H, *J* = 7.72 Hz, *J* = 0.92 Hz, H_1), 8.18 (dt, 2H, *J* = 8.19 Hz, *J* = 0.85 Hz, H_4), 7.84 (dt, 4H, *J* = 7.54 Hz, *J* = 0.96 Hz, H_5), 7.71-7.74 (m, 6H, H_8 and H_3), 7.52 (d, 2H, *J* = 8.10 Hz, H_9), 7.47 (td, 2H, *J* = 7.44 Hz, *J* = 0.95 Hz, H_2), 7.43 (dt, 2H, *J* = 7.64 Hz, *J* = 0.91 Hz, H_{12}), 7.12 (td, 4H, *J* = 7.37 Hz, *J* = 1.16 Hz, H_6), 7.08 (td, 4H, *J* = 7.36 Hz, *J* = 1.12 Hz, H_7), 6.79 (td, 2H, *J* = 7.37 Hz, *J* = 0.93 Hz, H_{10}), 6.68 (td, 2H, *J* = 7.42 Hz, *J* = 1.24 Hz, H_{11}). **^{13}C NMR** (151 MHz, DMSO-d_6) δ 145.7, 144.9, 139.9, 138.5, 137.6, 136.4, 126.8, 125.4, 124.2, 123.6, 123.3, 122.8, 121.9, 121.3, 121.0, 120.5, 120.2, 119.4, 116.7, 112.3, 111.1, 111.0, 110.9. **HRASAP-MS** *m/z* = 789.2725 $[M+H]^+$ (calculated for $C_{56}H_{33}N_6$ = 789.2766).

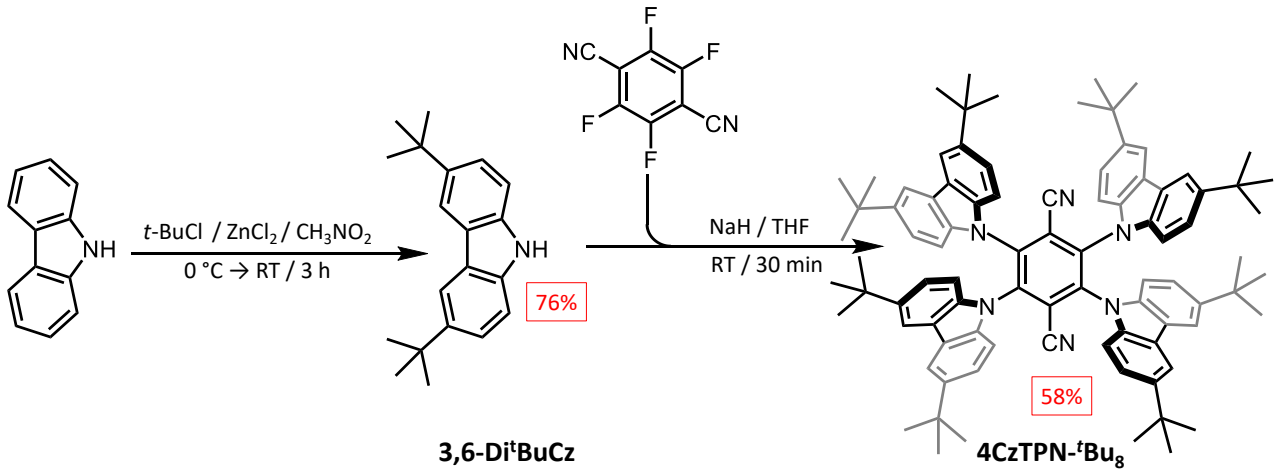

Scheme S2 The synthetic route used to prepare **4CzTPN-^{t}Bu$_8$.**

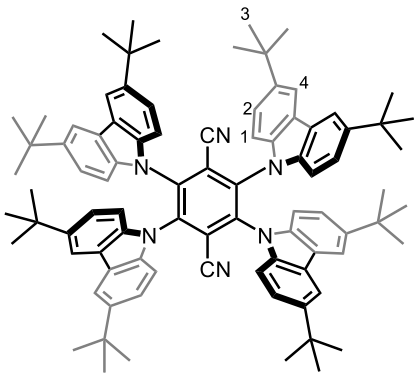

4CzTPN-^{t}Bu$_8$: Anhydrous sodium hydride (0.45 g, 18.70 mmol) was added to the stirred solution of **3,6-di-*tert*-butyl-carbazole** (3.50 g, 12.00 mmol) in anhydrous THF (50 mL). The mixture was stirred for 30 min at RT and then tetrafluoroterephthalonitrile (0.50 g, 2.89 mmol) was added. The mixture was stirred overnight at RT and then quenched into H_2O and EtOH. The crude product was filtered and washed with EtOH and CH_2Cl_2 give the title compound as an orange solid (2.10 g, 1.66 mmol, 58%). **M.P.** >400 °C. **^{1}H NMR** (700 Hz, $CDCl_3$) δ 7.47 (d, 8H, J = 1.82 Hz, H_4), 7.03 (dd, 8H, J = 8.43 Hz, J = 1.87 Hz, H_1), 6.97 (d, 8H, J = 8.40 Hz, H_2), 1.38 (s, 72H, H_3). **^{13}C NMR** (176 Hz, $CDCl_3$) δ 144.6, 138.7, 137.0, 124.9, 123.2, 121.8, 116.0, 109.5, 34.8, 32.0. **LRMS-MALDI-TOF** *m/z* = 1236.0 $[M-H]^+$ (calculated for $C_{88}H_{96}N_6$ = 1236.77).

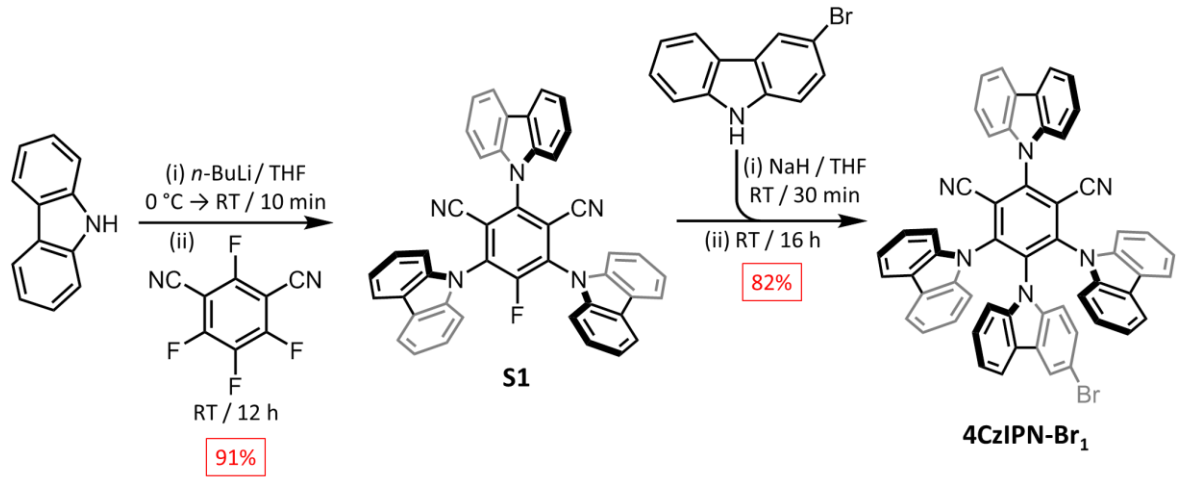

Scheme S3 The synthetic route used to prepare **4CzIPN-Br$_1$.**

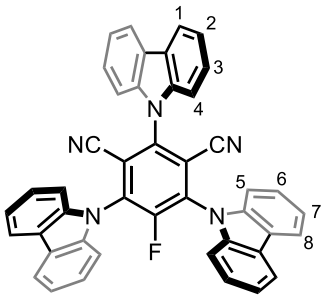

S1: Carbazole (627 mg, 3.75 mmol) was placed into an oven-dried round-bottomed flask fitted with a septum under a N_2 atmosphere. Anhydrous THF (15 mL) was added and the resulting solution was cooled to 0 °C before adding *n*-BuLi (1.58 mL, 3.94 mmol, 2.5 M in hexanes) and stirring for 10 min as the solution was warmed to RT. The lithium carbazolide formed *in situ* precipitated from solution. A solution of tetrafluoroisophthalonitrile (250 mg, 1.25 mmol) in anhydrous THF (5 mL) was added to the suspension of lithium carbazolide, and the mixture stirred at rt for 12 h. The resulting solution was then poured into water (150 mL), causing a yellow precipitate to form. The solid was isolated by filtration, washing on the filter with water (2 × 10 mL), then dissolved in EtOAc (100 mL), dried over $MgSO_4$ and filtered. The solvent was removed under reduced pressure and the crude residue was purified by column chromatography (Teledyne Isco CombiFlash Rf+ system, 80 g SiO_2, hexanes−EtOAc, gradient elution) to yield the title compound as a yellow solid (733 mg, 1.14 mmol, 91%). **M.P.** 188 – 190 °C. **^{1}H NMR** (700 MHz, $CDCl_3$) δ 8.19 (dt, *J* = 7.7, 1.0 Hz, 2H, H_1), 8.15 (dt, *J* = 7.7, 0.9 Hz, 4H, H_8), 7.61 (ddd, *J* = 8.3, 7.3, 1.2 Hz, 2H, H_3), 7.56 (ddd, *J* = 8.4, 7.3, 1.2 Hz, 4H, H_6), 7.45 (td, *J* = 7.5, 0.9 Hz, 2H, H_2), 7.43 – 7.38 (m, 6H, H_4 and H_7), 7.35 (d, *J* = 8.4 Hz, 4H, H_5). **^{13}C NMR** (101 MHz, $CDCl_3$) δ 142.6 (d, J_{CF} = 4.3 Hz), 140.2, 139.3, 135.3 (d, J_{CF} = 14.5 Hz), 127.2, 127.0, 125.0, 124.8, 122.6, 122.4, 121.5, 121.2, 115.4 (d, J_{CF} = 2.9 Hz), 111.0 (d, J_{CF} = 3.2 Hz), 109.9, 109.9, 109.3. **HRASAP-MS** *m/z* = 642.2064 $[M+H]^+$ (calculated for $C_{44}H_{25}FN_5$ = 642.7172).

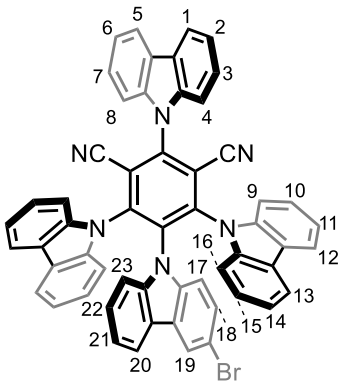

4CzIPN-Br$_1$: **3-Bromocarbazole** (92 mg, 373 µmol) was dissolved in anhydrous THF (10 mL) in an oven-dried round-bottomed flask fitted with a septum under a N_2 atmosphere. A 60% dispersion of NaH in mineral oil (18.3 mg, 466 µmol) was added and the mixture stirred for 30 min at RT. **S1** (200 mg, 311 µmol) was then added and the mixture stirred at RT for 16 h. The reaction was quenched by the addition of water (100 mL), then extracted with EtOAc (3 × 100 mL). The combined organic extracts were dried over $MgSO_4$, filtered and the solvent removed under reduced pressure. The crude residue was purified by column chromatography (Teledyne Isco CombiFlash Rf+ system, 80 g SiO_2, hexanes−EtOAc, gradient elution) to yield the title compound as a yellow solid (221 mg, 243 µmol, 82%). **M.P.** >350 °C. **^{1}H NMR** (700 MHz, $CDCl_3$) δ 8.22 (d, *J* = 7.7 Hz, 1H, H_1 and H_5), 7.76 – 7.67 (m, 8H, H_3, H_4, H_7, H_8, H_{12}, and H_{13}), 7.49 (ddd, *J* = 7.8, 6.8, 1.3 Hz, 2H, H_2 and H_6), 7.45 (s, 1H, H_{19}), 7.27 (d, *J* = 7.4 Hz, 1H, H_{20}), 7.21 (d, *J* = 8.1 Hz, 2H, H_9 or H_{16}), 7.20 – 7.18 (m, 2H, H_9 or H_{16}), 7.15 – 7.06 (m, 8H, H_{10}, H_{11}, H_{14}, and H_{15}), 6.84 – 6.81 (m, 2H, H_{21} and H_{23}), 6.74 – 6.72 (m, 2H, H_{17} and H_{18}), 6.65 (ddd, *J* = 8.2, 7.2, 1.2 Hz, 1H, H_{22}). **^{13}C NMR** (176 MHz, $CDCl_3$) δ 145.3, 145.1, 140.1, 140.0, 138.3, 138.2, 137.5, 136.0, 134.3, 127.4, 127.1, 127.1, 126.0, 126.0, 125.8, 125.7, 125.1, 125.1, 124.7, 124.7, 122.8, 122.7, 122.6, 122.3, 122.2, 121.6, 121.5, 121.5, 120.7, 120.7, 112.0, 116.5, 114.0, 111.7, 110.9, 110.0, 109.9, 109.8, 109.6, 109.6. **HRASAP-MS** *m/z* = 866.1819 $[M]^+$ (calculated for $C_{56}H_{31}BrN_6$ = 866.1794).

3. ^{1}H and ^{13}C NMR spectroscopic characterisation of synthesized compounds

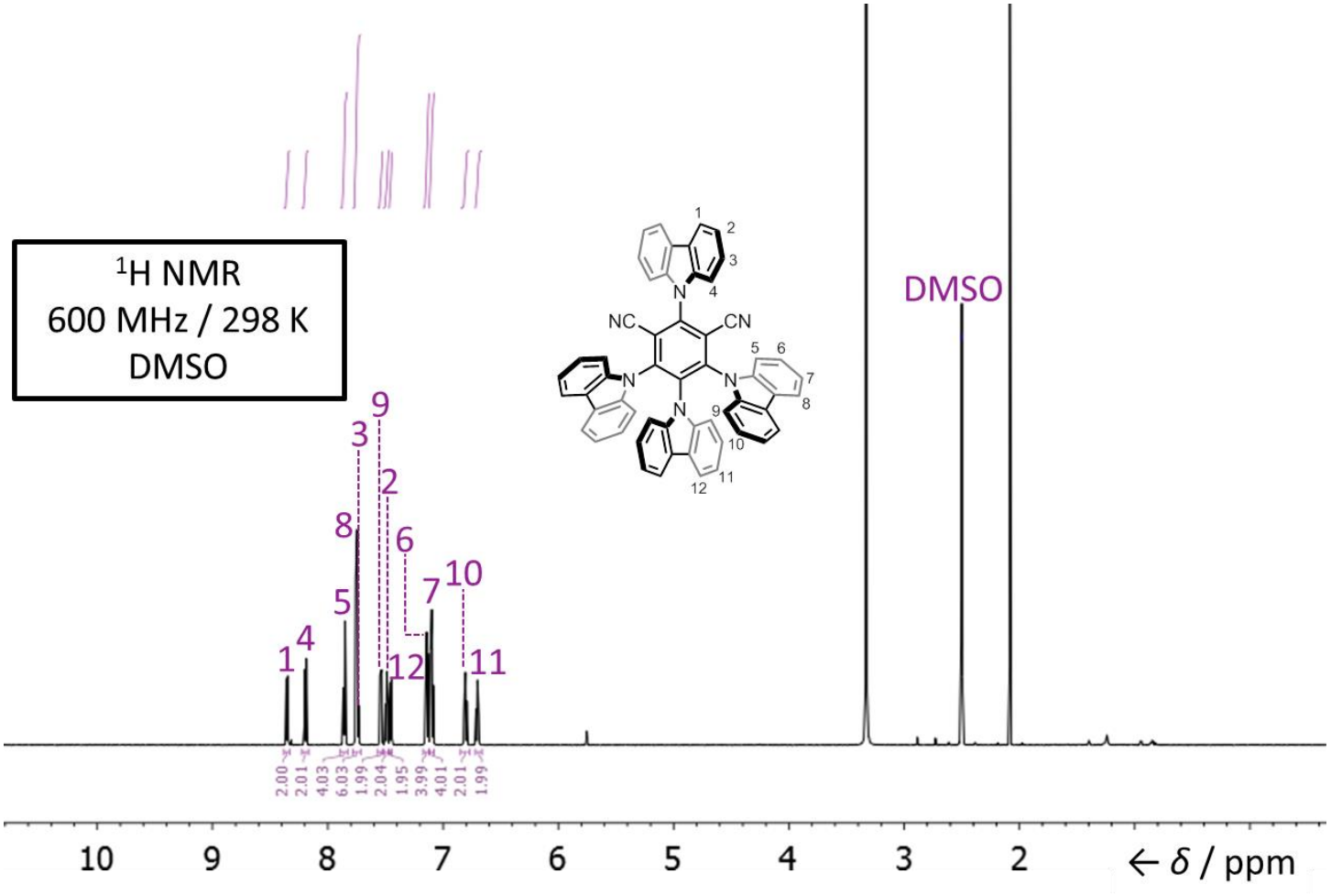

Figure S1 ^{1}H NMR Spectrum of **4CzIPN.**

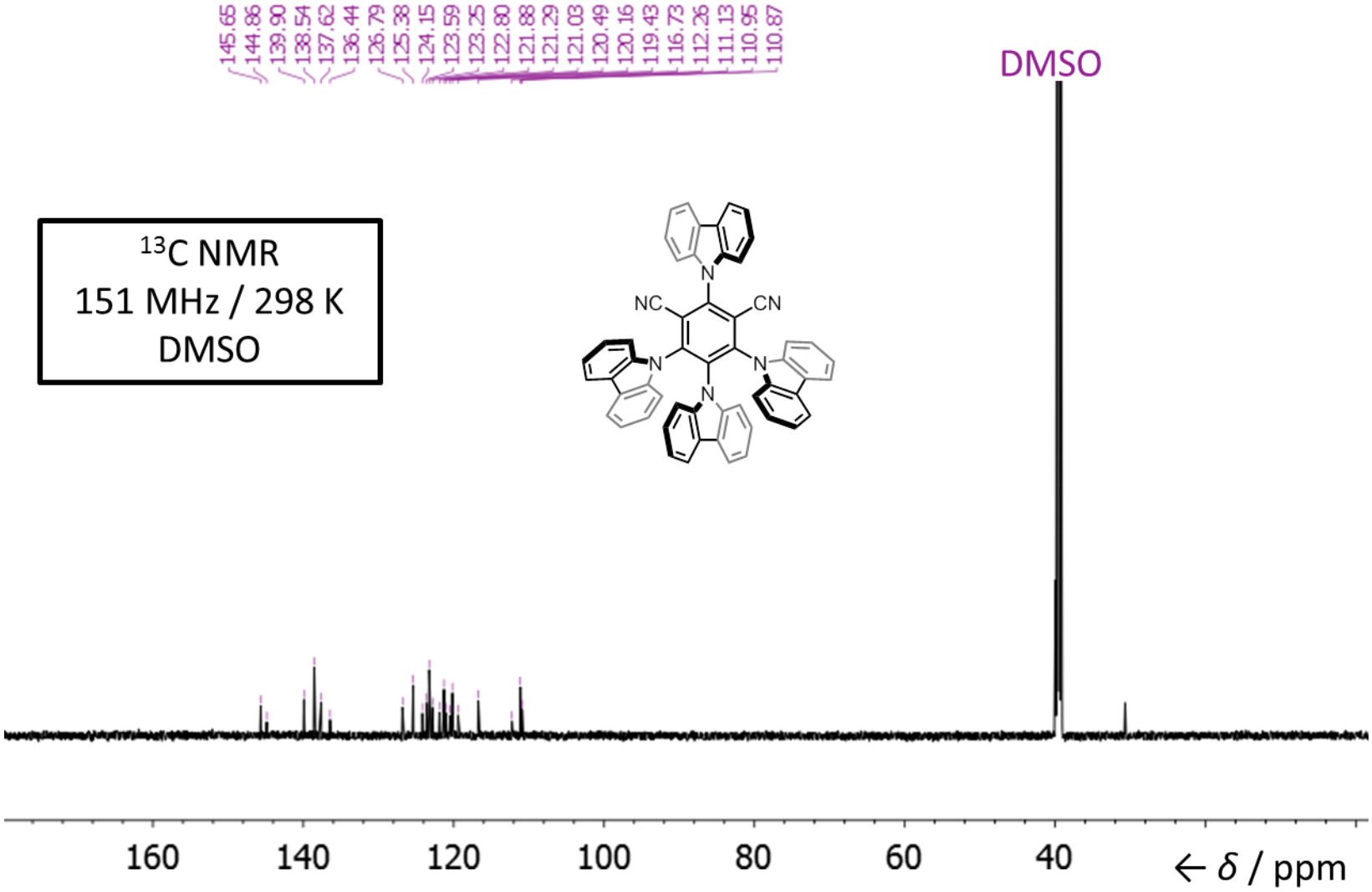

Figure S2 ^{13}C NMR Spectrum of **4CzIPN.**

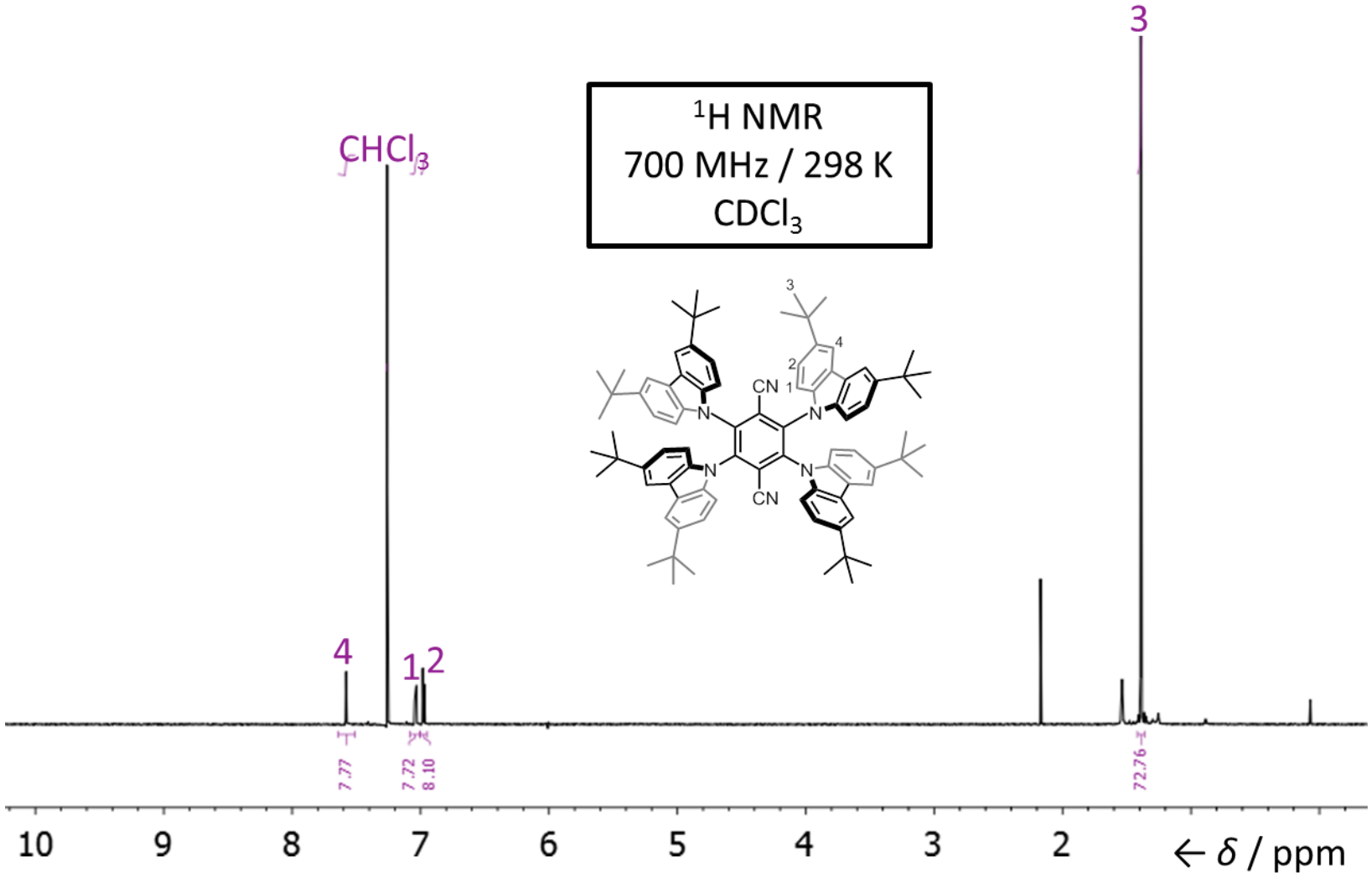

Figure S3 ^{1}H NMR Spectrum of **4CzTPN-^{t}Bu$_8$.**

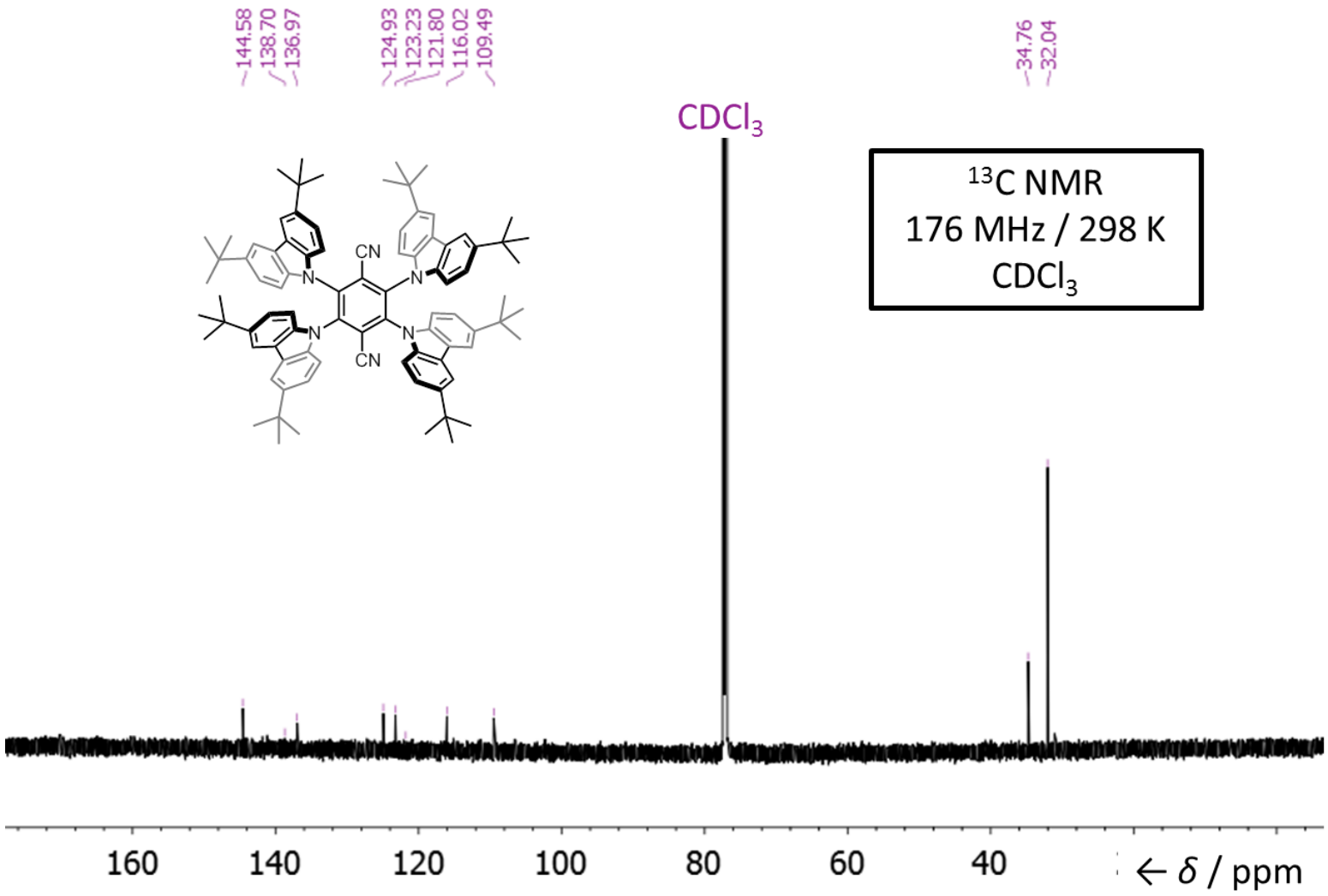

Figure S4 ^{13}C NMR Spectrum of **4CzTPN-^{t}Bu$_8$.**

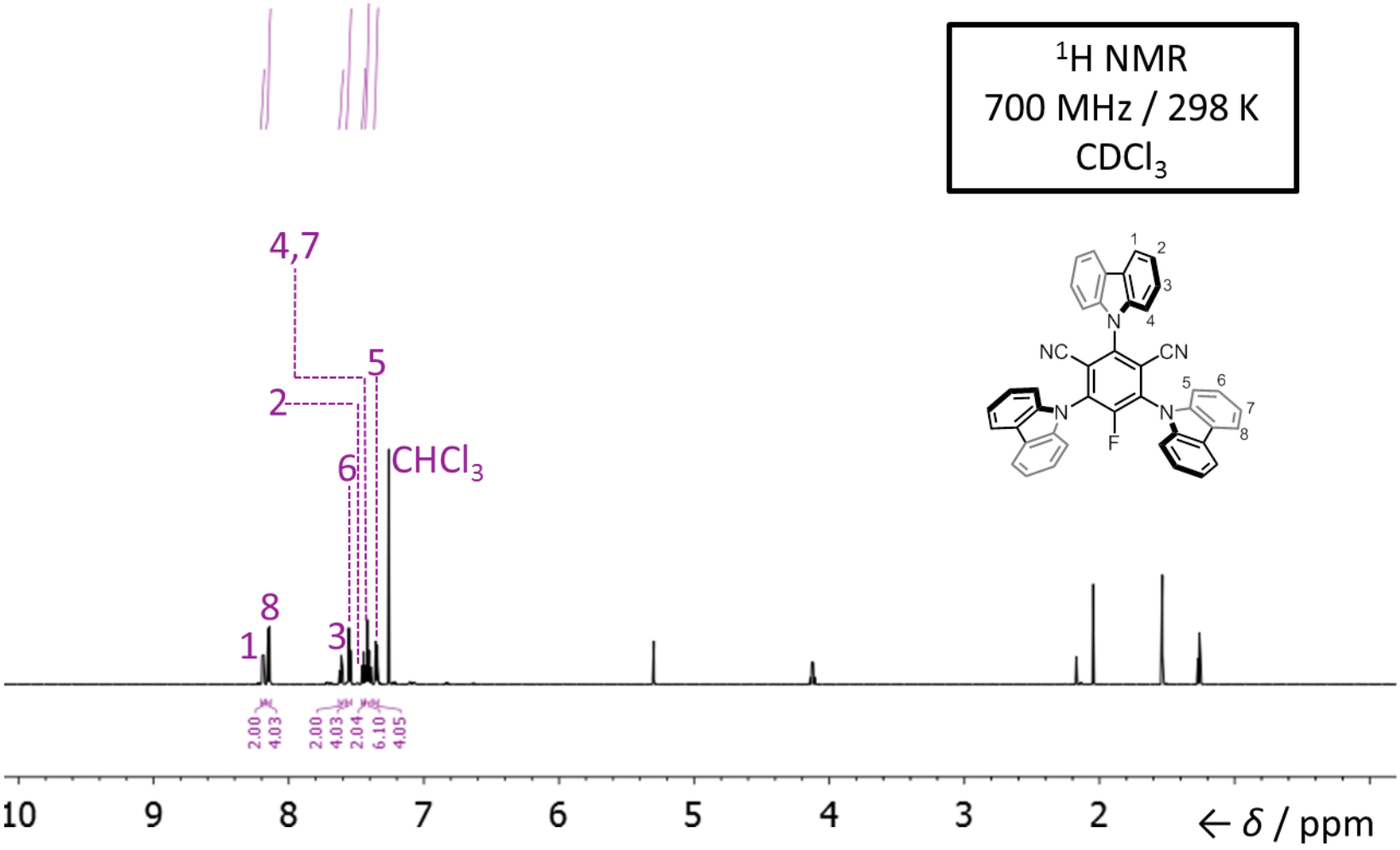

Figure S5 ^{1}H NMR Spectrum of **S1.**

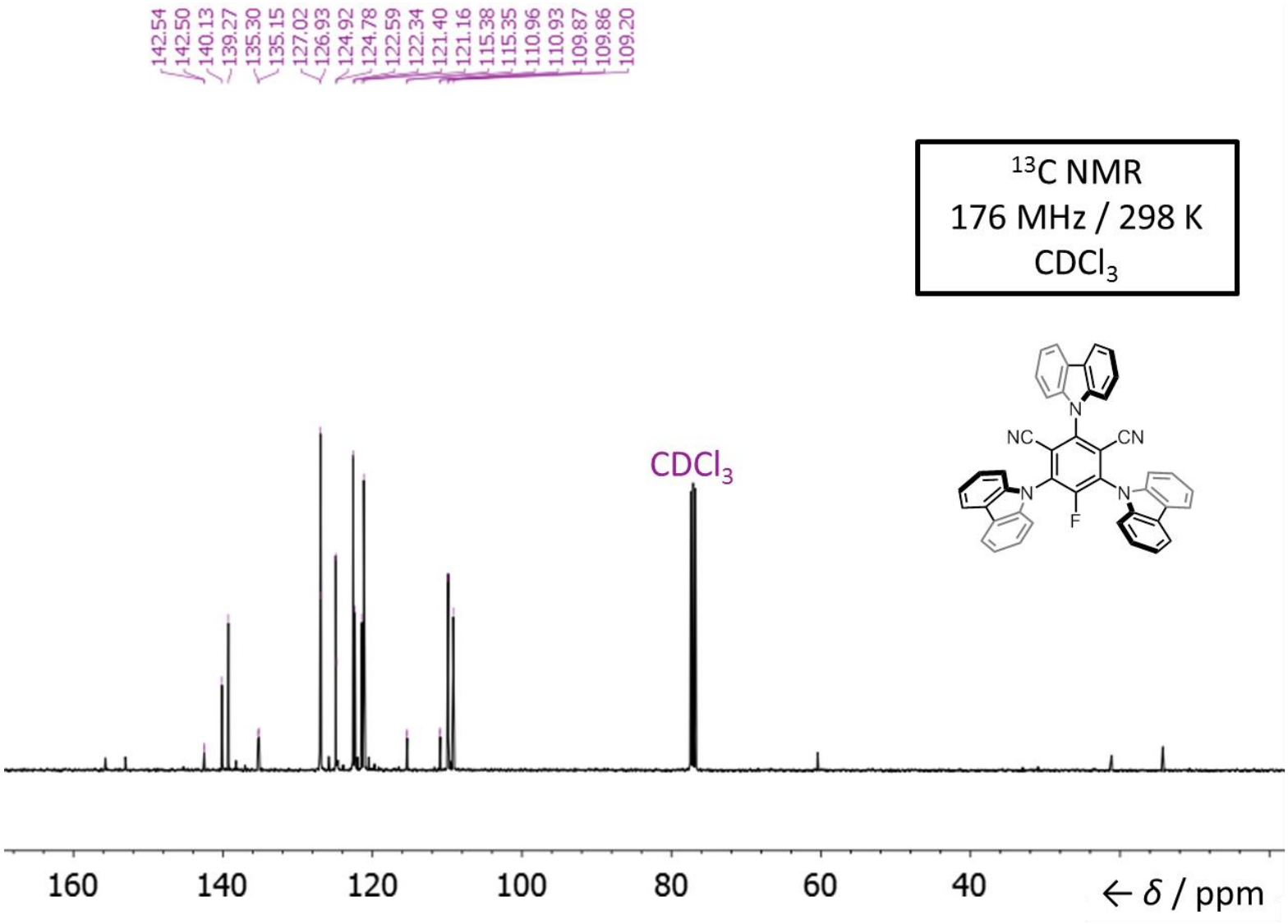

Figure S6 ^{13}C NMR Spectrum of **S1.**

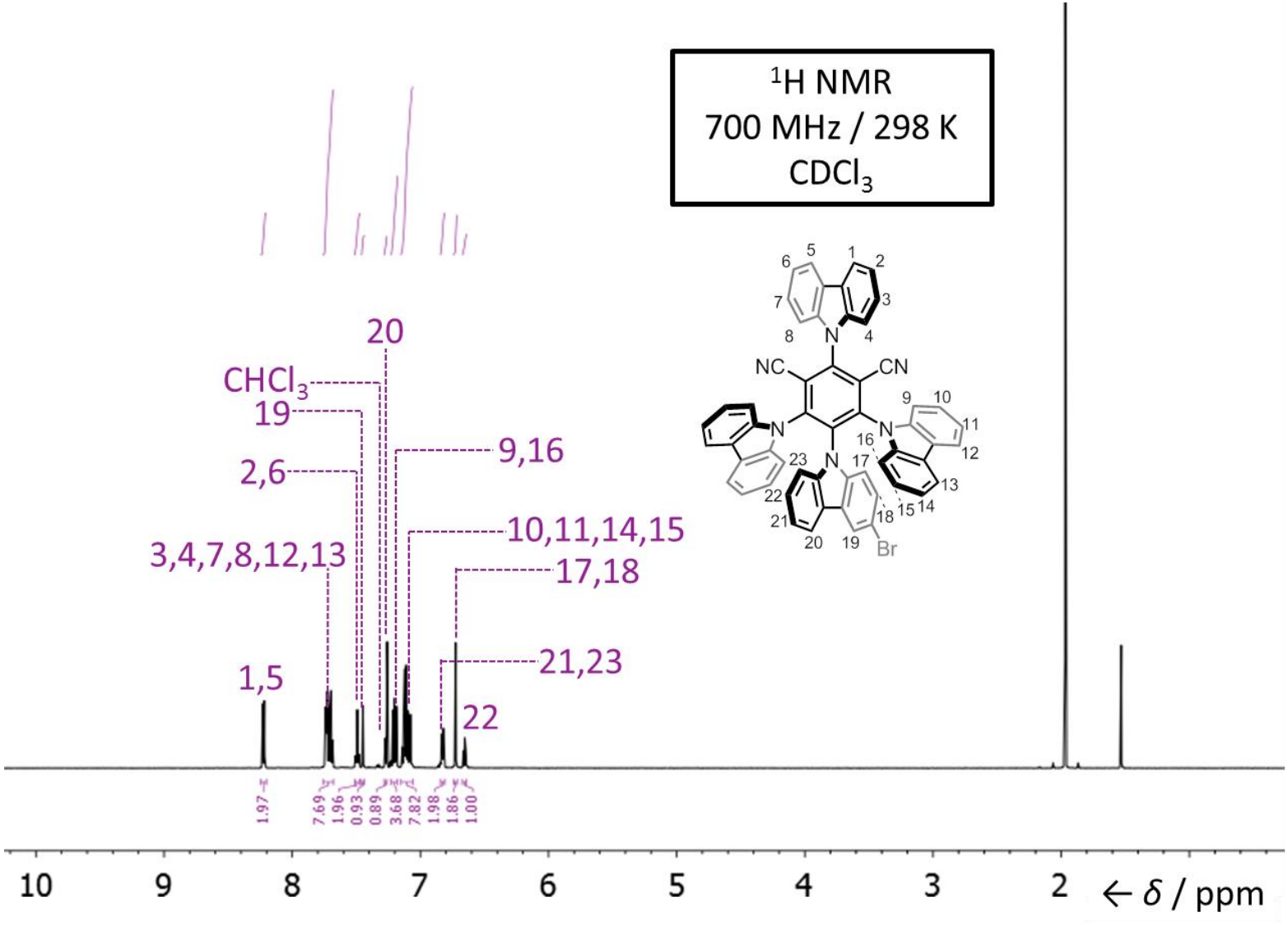

Figure S7 ^{1}H NMR Spectrum of **4CzIPN-Br$_1$.**

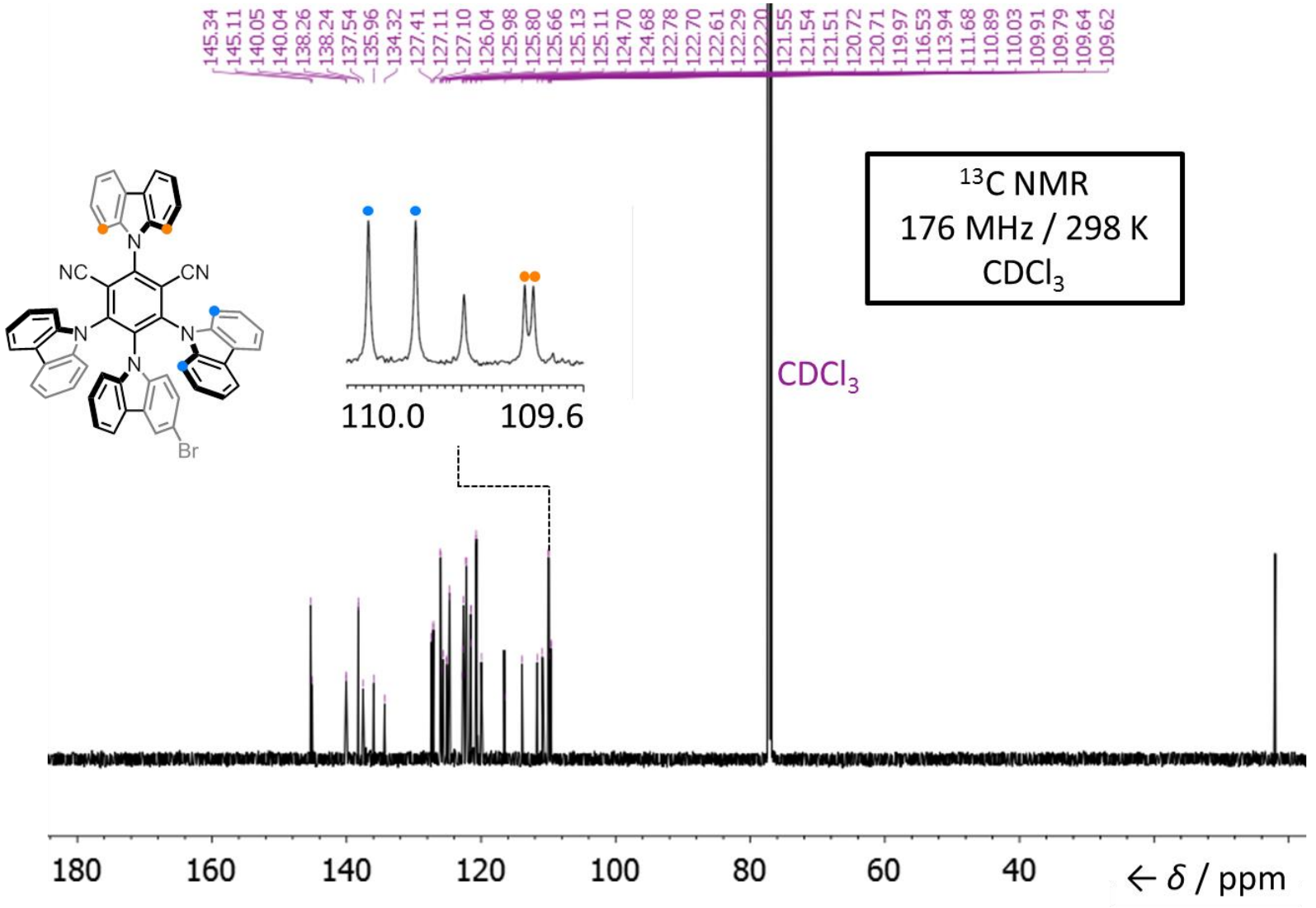

Figure S8 ^{13}C NMR Spectrum of **4CzIPN-Br$_1$**

4. Photoluminescence (PL) spectroscopy of dilute solutions and crystals

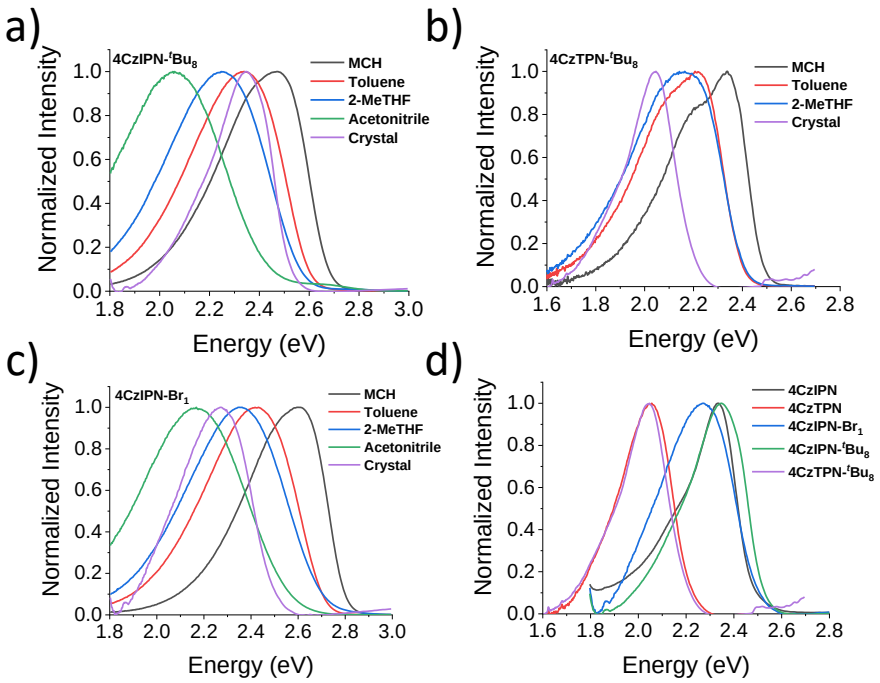

Figure S9 Solvatochromism and crystal emission of **4CzIPN-^{t}Bu$_8$, 4CzTPN-^{t}Bu$_8$** and **4CzIPN-Br$_1$.** The emission of the crystal for each molecule is significantly redshifted and of narrower linewidth. (**a**) The sublimed crystal of **4CzIPN-^{t}Bu$_8$** has an emission peak like the molecule in a dilute (20 µM) toluene solution. (**b**) The emission of the sublimed crystal of **4CzTPN-^{t}Bu$_8$** is redshifted compared to its emission in 2-MeTHF solution. (**c**) For the solvent-grown crystals of **4CzIPN-Br$_1$** the emission profile is between that of 2-MeTHF and Acetonitrile. (**d**) The emission of the crystals for the studied molecules showing that the addition of the *tert*-butyl groups has very little influence in the prevention of dimer formation.

5. Powder and solution of 4CzTPN in DMSO

a) b)

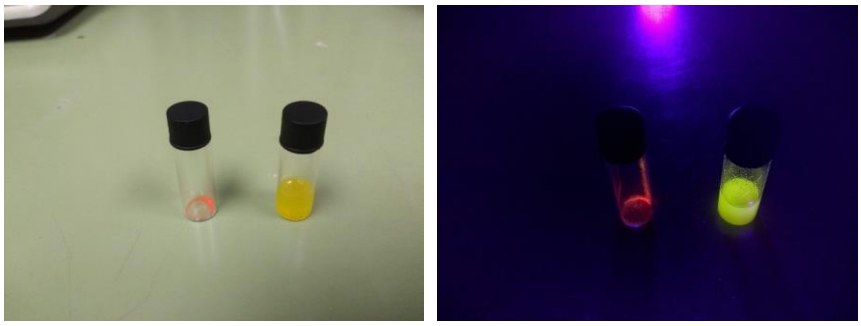

Figure S10 The change in emission between **4CzTPN** crystals in air and in dimethylsulfoxide (DMSO). **4CzTPN** in air and in DMSO (**a**) under room light and (**b**) under UV light. The blue shift of the absorption and emission bands of this molecule on dissolving in an extremely polar solvent indicates that these colour changes cannot be attributed to polarity alone.

6. Variable temperature (VT) NMR spectroscopy

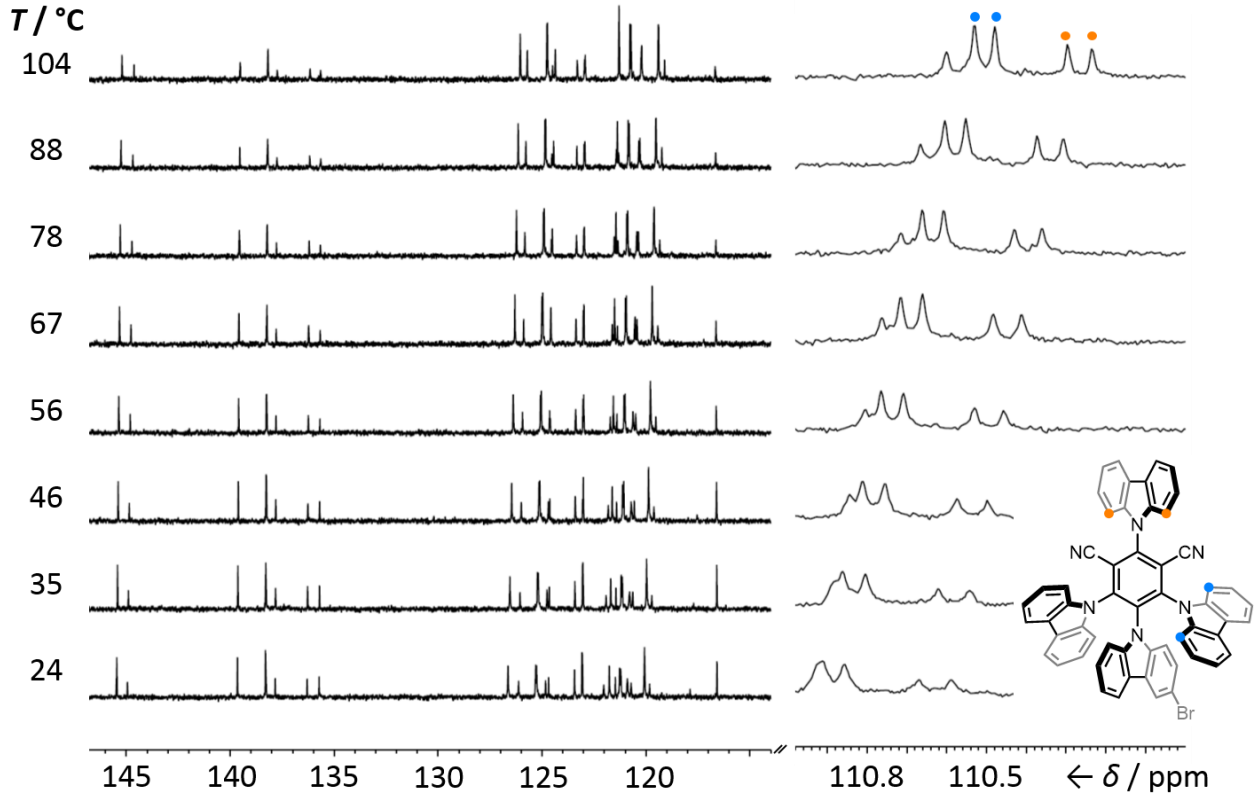

Figure S11 Partial ^{13}C NMR spectra, 126 MHz, of a $(CD_3)_2SO$ solution of **4CzIPN-Br$_1$** from 24 °C to 104 °C. Two pairs of peaks are labelled, which each correspond to a set of non-equivalent sites that would undergo exchange upon 180° rotation of a carbazole group relative to the central benzene ring. The resonances do not coalesce at high temperature – they remain in slow exchange, even at 104 °C.

The plane of symmetry passing through the central benzene C-atoms of **4CzIPN**, **4CzTPN**, **4CzIPN-^{t}Bu$_8$** and **4CzTPN-^{t}Bu$_8$** is absent in **4CzIPN-Br$_1$**. Therefore, there are more distinct nuclear environments observed in the NMR spectrum of **4CzIPN-Br$_1$**. In slow exchange, i.e., when 180° rotation around the C–N bonds connecting the central benzene to the carbazole groups occurs at a rate lower than the frequency difference between exchanging sites, one would expect to observe up to 41 discrete ^{13}C resonances. In fast exchange, as few as 29 discrete ^{13}C resonances would be observed. There are 39 observable resonances present (Figure S11) in the ^{13}C NMR spectra of a $(CD_3)_2SO$ solution of **4CzIPN-Br$_1$** over the temperature range of 24 – 104 °C, indicating that exchange by rotation is slow. Resonances that have been identified (coloured dots, Figure S11) as arising from exchangeable sites show no sign of approaching coalescence, even at 104 °C. Using the equation:

$$k_c = \frac{\pi}{\sqrt{2}}\Delta\nu$$

where k_c is the coalescence rate constant and $\Delta\nu$ is the difference in frequency between a pair of exchangeable resonances (blue dots, Figure S11), we approximate k_c of 28.9 Hz, if the sites were to reach the coalescence temperature. This allows us to estimate a lower limit for the free energy of activation, $\Delta G^{\ddagger}$, using the equation:

$$\Delta G^{\ddagger} = -RT\ln\frac{k_c h}{k_B T}$$

where R is the gas constant, T is temperature and k_B is Boltzmann's constant, with a value of 377 K for the temperature. Therefore, $\Delta G^{\ddagger}$ for rotation of the carbazole rings present in **4CzIPN-Br$_1$** is >87 kJ·mol^{-1}.

7. Decay fits of 532 nm excited zeonex film

Table S1 The fitting parameters for the photoluminescence decays of the **4CzIPN** at 10 wt% in zeonex, excited at 532 nm**.** The R^2 values for the fits are 0.99009 and 0.98096 for the PF and DF RT fits, and 0.99072 and 0.98221 for the PF and DF 80 K fits.

Temperature	aLP	τLP	aPF/CT(D)	τPF/CT(D)	aDF/CT(D)	τDF/CT(D)
RT	7.04E6 ± 0.76E6	6.90 ± 0.93	2.06E6 ± 0.26E6	40.0 ± 3.0	2.95E4 ± 0.09E4	2.73E3 ± 0.12E3
80 K	4.46E6 ± 1.00E6	4.56 ± 0.93	1.94E6 ± 0.15E6	35.0 ± 1.8	8.70E3 ± 0.22E3	4.88E3 ± 0.20E3

8. PL spectroscopy of zeonex films and methylcyclohexane solution

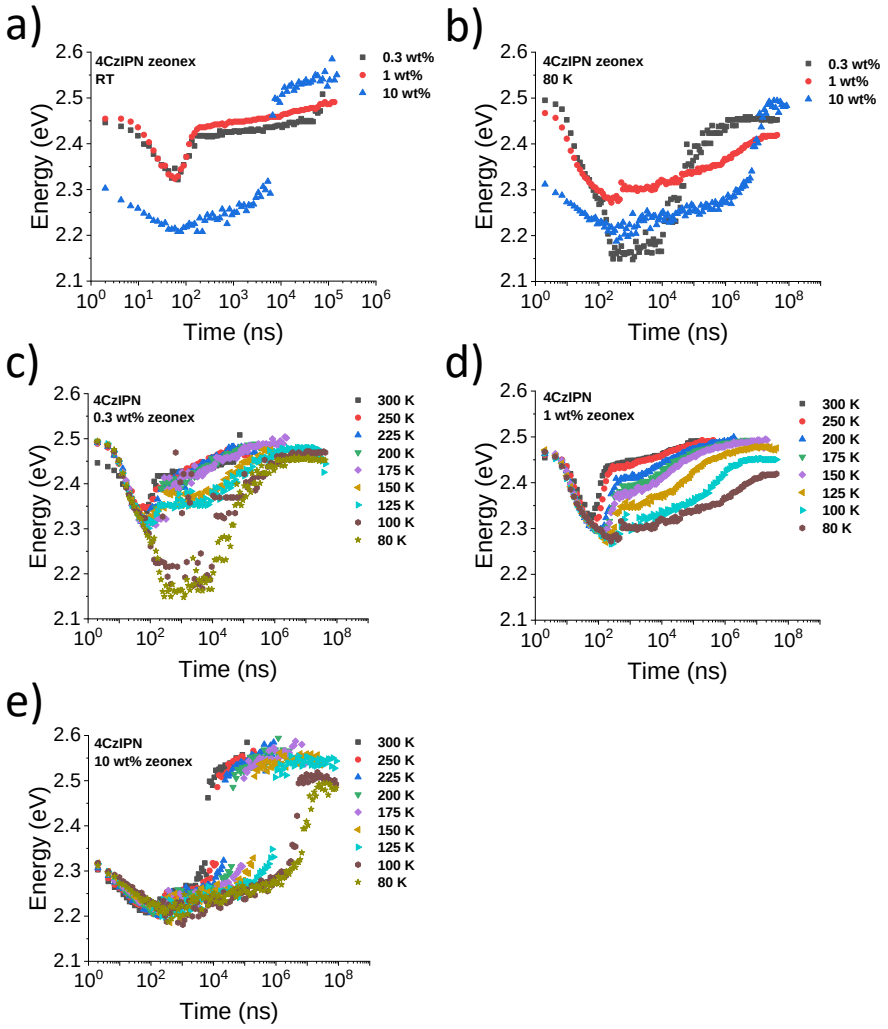

Figure S12 The shift of the peak emission energy as a function of time in the doped zeonex films. (**a**) Comparing the three concentrations the 10 wt% film starts at a redshifted value and stays at that value until some monomer delayed emission reappears at 10^4 ns. (**b**) On cooling to 80 K, the monomer TADF is reduced and all the films take longer to return to the higher energy states as the dimer emission begins to dominate. (**c**) In the 0.3 wt% film there is very little dimer contribution demonstrated by the very small energy shifts. The large shifts at 100 K and 80 K are most likely due to the small-signal-to-noise ratio overemphasising the shift in that region. (**d**) In the 1 wt% film there is a more significant contribution from the dimer, shown by the shift in energies to below 2.3 eV. However, the prompt emission and TADF are predominantly from the monomer. (**e**) The 10 wt% film has the largest dimer contribution both in the prompt and delayed emission due to the significant red shifts compared to the 0.3 wt% and 1 wt% films. At longer times the monomer TADF or phosphorescence returns and is the reason for the associated blue shift.

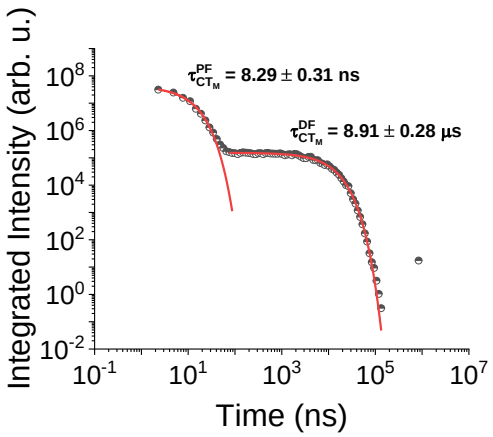

Figure S13 Decays of the time-resolved emission of **4CzIPN** in methylcyclohexane. The decay fit parameters are found in Table S2.

Table S2 The fitting parameters for the photoluminescence decay of **4CzIPN** in a degassed methylcyclohexane solution. The R^2 values for the fits are 0.98721 and 0.99033 for the PF and DF at RT.

Temperature	**aPF/CT(M)**	**τPF/CT(M)**	**aDF/CT(M)**	**τDF/CT(M)**
RT	4.17E7 ± 0.19E7	8.29 ± 0.31	1.53E5 ± 0.01E5	8.91E3 ± 0.28E3

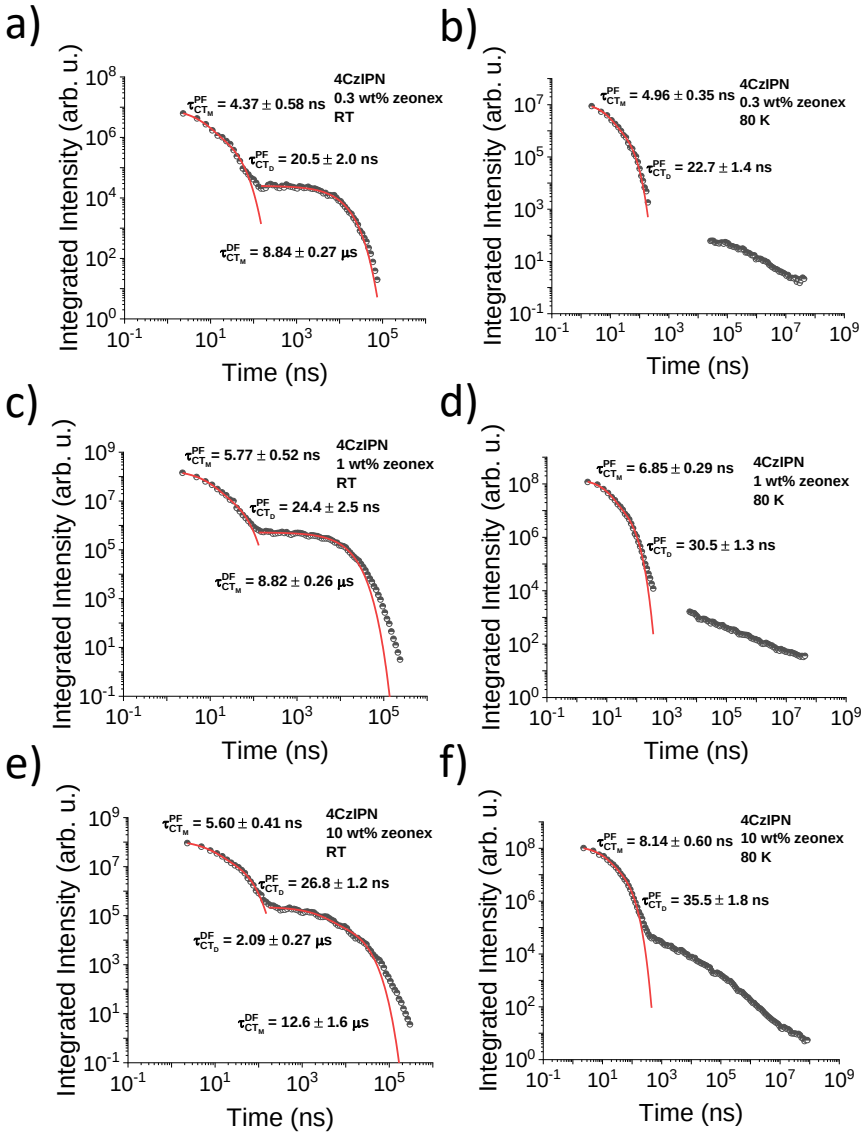

Figure S14 Decays of the time-resolved emission of **4CzIPN** in zeonex at varying concentrations at both RT and 80 K. (**a**) **4CzIPN** at 0.3 wt% in zeonex at RT. (**b**) **4CzIPN** at 0.3 wt% in zeonex at 80 K. (**c**) **4CzIPN** at 1 wt% in zeonex at RT. (**d**) **4CzIPN** at 1 wt% in zeonex at 80 K. (**e**) **4CzIPN** at 10 wt% in zeonex at RT (**f**) **4CzIPN** at 10 wt% in zeonex at 80 K. The decay fit parameters are found in Tables S3-5.

Table S3 The fitting parameters for the photoluminescence decays of the **4CzIPN** at 0.3 wt% in zeonex**.** The R^2 values for the fits are 0.98986 and 0.99 for the PF and DF RT fits, and 0.99607 for the 80 K fit.

Temperature	aPF/CT(M)	τPF/CT(M)	aPF/CT(D)	τPF/CT(D)	aDF/CT(M)	τDF/CT(M)
RT	7.57E6 ± 0.60E6	4.37 ± 0.58	2.04E6 ± 0.38E6	20.5 ± 2.0	2.51E4 ± 0.04E4	8.84E3 ± 0.27E3
80 K	1.02E7 ± 0.05E7	4.96 ± 0.35	2.38E6 ± 0.29E6	22.7 ± 1.4	-	-

Table S4 The fitting parameters for the photoluminescence decays of the **4CzIPN** at 1 wt% in zeonex. The R^2 values for the fits are 0.994 and 0.99052 for the PF and DF RT fits, and 0.99812 for the 80 K fit.

Temperature	aPF/CT(M)	τPF/CT(M)	aPF/CT(D)	τPF/CT(D)	aDF/CT(M)	τDF/CT(M)
RT	1.64E8 ± 0.08E8	5.77 ± 0.52	3.28E7 ± 0.68E7	24.4 ± 2.5	5.18E5 ± 0.08E5	8.82E3 ± 0.26E3
80 K	1.32E8 ± 0.03E8	6.85 ± 0.29	2.86E7 ± 0.24E7	30.5 ± 1.3	-	-

Table S5 The fitting parameters for the photoluminescence decays of the **4CzIPN** at 10 wt% in zeonex**.** The R^2 values for the fits are 0.99736 and 0.98213 for the PF and DF RT fits, and 0.99668 for the 80 K fit.

Temperature	aPF/CT(M)	τPF/CT(M)	aPF/CT(D)	τPF/CT(D)	aDF/CT(D)	τDF/CT(D)	aDF/CT(M)	τDF/CT(M)
RT	9.27E7 ± 0.39E7	5.60 ± 0.41	3.17E7 ± 0.28E7	26.8 ± 1.2	1.68E5 ± 0.11E5	2.09E3 ± 0.27E3	6.12E4 ± 1.15E4	1.26E4 ± 0.17E4
80 K	9.02E7 ± 0.37E7	8.14 ± 0.60	3.40E7 ± 0.33E6	35.5 ± 1.8	-	-	-	-

Table S6 The PLQYs and natural lifetimes of the monomer and dimer species.

Material	Measured Lifetime (µs)	Quantum Yield	Natural Lifetime (µs)
4CzIPN Dimer (Pristine film)	2.05	0.34	6.03
4CzIPN Dimer (10 wt% film)	2.1	0.26	8.07
4CzIPN Monomer (1 wt% Film)	8.8	0.87	10.1
4CzIPN Monomer (Annealed Film)	0.5	0.17	2.94

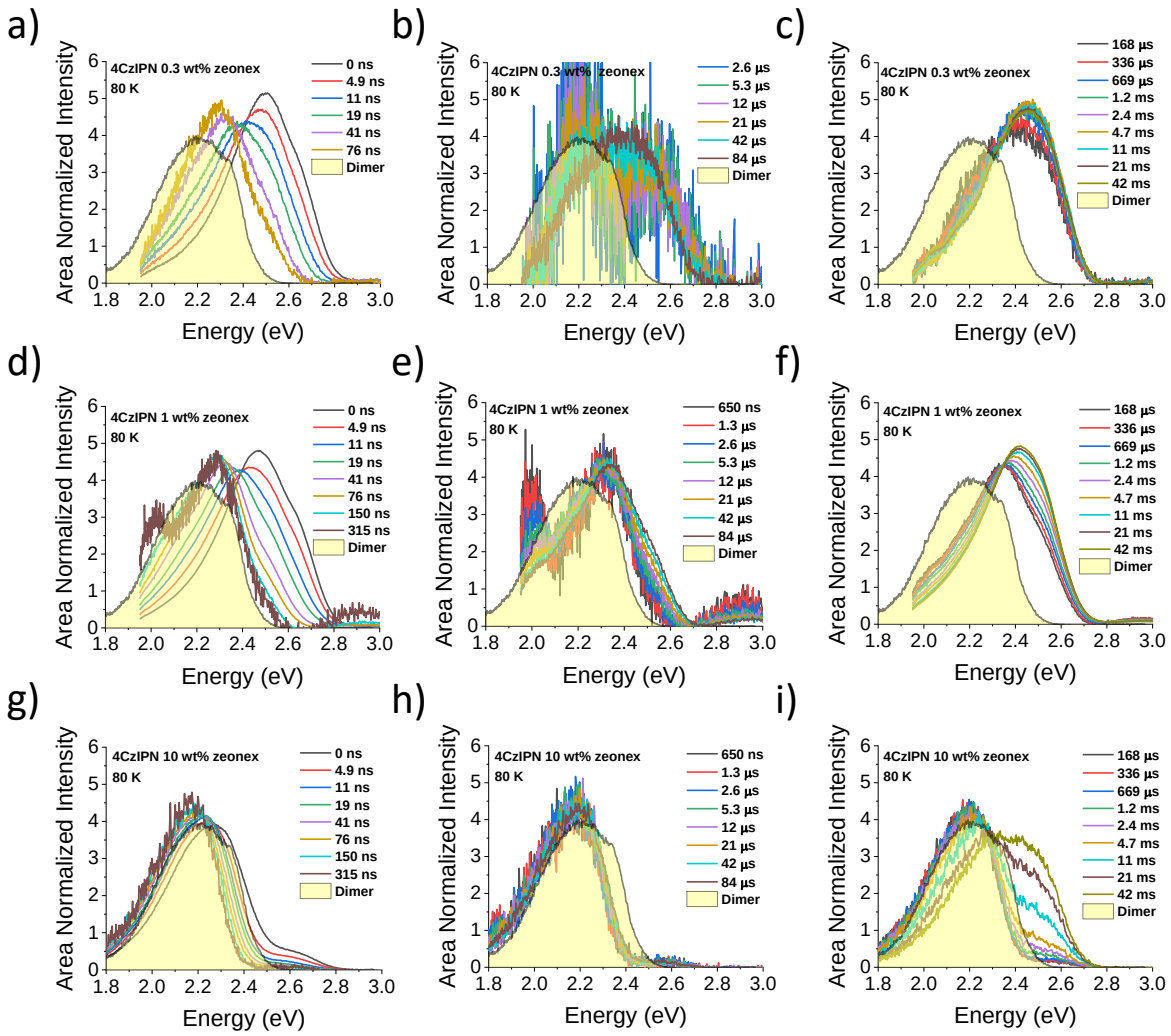

Figure S15 80 K time-resolved spectra of the doped **4CzIPN**:zeonex films**.** (**a**-**c**) The time-resolved emission of the 0.3 wt% doped **4CzIPN**:zeonex film which predominantly has monomer emission both in the prompt and delayed time regions. Due to very little dimer formation the intensity during the delayed fluorescence region (**b**) is significantly reduced due to the larger singlet-triplet gap for the monomer species in zeonex. At longer times (**c**) the emission is dominated by the monomer phosphorescence with onset 2.7 eV. For the 1 wt% film (**d-f**) the trend is similar however the red shift is more significant in the intermediate time ranges (**e**), which is attributed to the dimer. At long times the monomer phosphorescence again returns. For the 10 wt% film (**g-i**) the emission at prompt and intermediate times is dominated by the dimer emission, it is only at long times that some of the monomer phosphorescence returns.

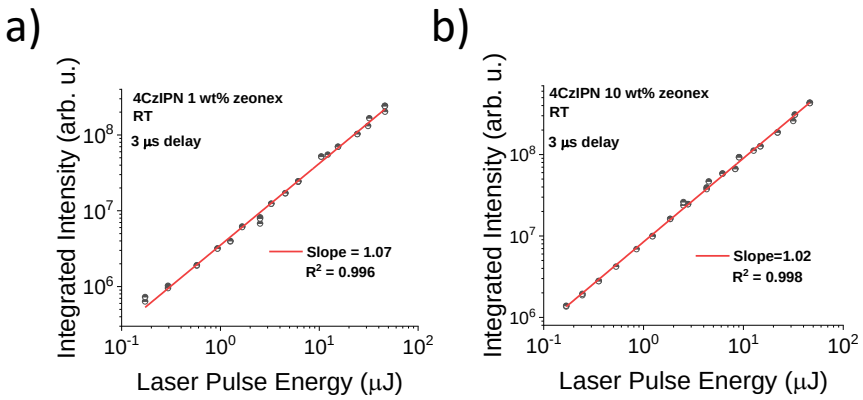

Figure S16 The laser energy dependence of **4CzIPN** in zeonex host films at 300 K. (**a**) The energy dependence of **4CzIPN** in a zeonex film at 1 wt% and at 3 μs delay. (**b**) The energy dependence of **4CzIPN** in a zeonex film at 10 wt% and at 3 μs delay. The slopes of close to 1 implies that they are monomolecular processes, which combined with the temperature dependence confirm TADF.

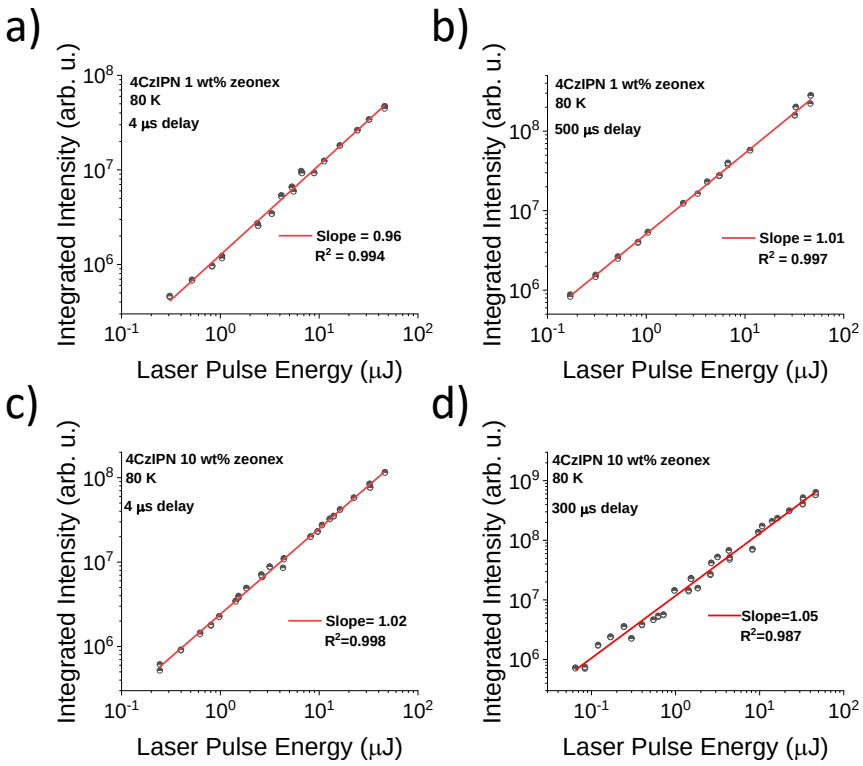

Figure S17 The laser energy dependence of **4CzIPN** in zeonex host films at 80 K. (**a**) The energy dependence of **4CzIPN** in a zeonex film at 1 wt% and at 4 μs delay. (**b**) The energy dependence of **4CzIPN** in a zeonex film at 1 wt% and at 500 μs delay. (**c**) The energy dependence of **4CzIPN** in a zeonex film at 10 wt% and at 4 μs delay. (**d**) The energy dependence of **4CzIPN** in a zeonex film at 10 wt% and at 300 μs delay. The slopes of close to 1 implies that they are monomolecular process, which combined with the temperature dependence confirms TADF.

9. Evaporated films and device physics

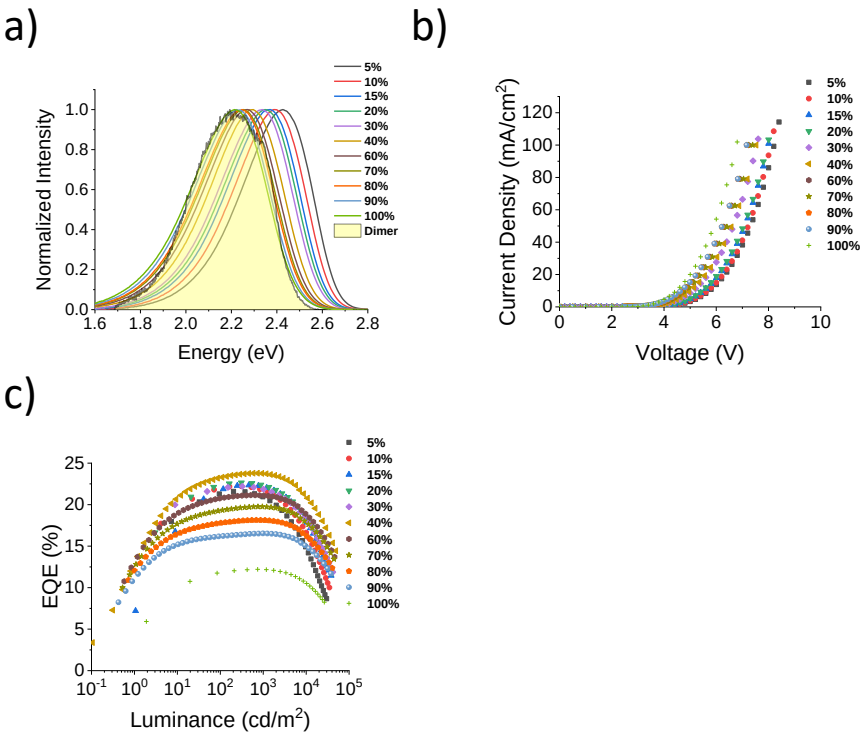

Figure S18 Device properties of **4CzIPN** based OLEDs with different concentrations of **4CzIPN** in the emissive layer of host mCBP. (**a**) Electroluminescence spectra, (**b**) JV curve and (**c**) EQE curve as a function of concentration.

10. PL spectroscopy of neat films of 4CzIPN

Table S7 The fitting parameters for the photoluminescence decays of a pristine neat **4CzIPN** drop cast film. The R^2 values for the fits are 0.99636 and 0.99753 for the PF and DF RT fits, and 0.99628 for the 80 K fit.

Temperature	aPF/CT(M)	τPF/CT(M)	aPF/CT(D)	τPF/CT(D)	aDF/CT(M)	τDF/CT(M)	aDF/CT(D)	τDF/CT(D)
RT	2.75E7 ± 0.11E7	7.85 ± 0.57	5.95E6 ± 1.01E6	33.6 ± 3.0	1.09E ± 0.05E5	388 ± 39	1.07E5 ± 0.05E5	2.05E3 ± 0.06E3
80 K	2.33E7 ± 0.11E7	5.16 ± 0.41	9.32E6 ± 0.69E6	26.2 ± 1.08	-	-	-	-

Table S8 The fitting parameters for the photoluminescence decays of an annealed neat **4CzIPN** drop cast film. The R^2 values for the fits are 0.99899 and 0.99094 for the PF and DF room temperature (RT) fits, and 0.99263 for the 80 K fit.

Temperature	aPF/CT(M)	τPF/CT(M)	aPF/CT(D)	τPF/CT(D)	aDF/CT(M)	τDF/CT(M)	aDF/CT(D)	τDF/CT(D)
RT	3.04E7 ± 0.16E7	2.01 ± 0.12	2.47E6 ± 0.39E6	18.6 ± 3.5	7.51E5 ± 0.12E5	536 ± 13	-	-
80 K	2.73E7 ± 0.16E7	3.76 ± 0.30	3.06E6 ± 0.66E6	18.9 ± 2.2	-	-	-	-

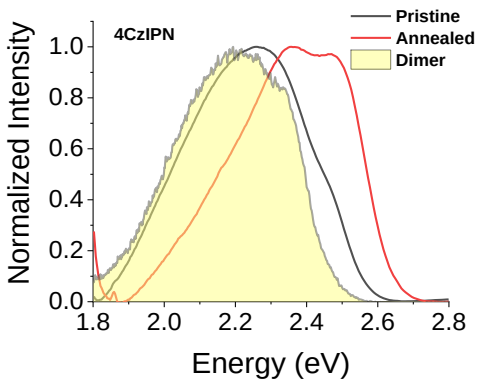

Figure S19 The effect of thermal annealing on the emission of **4CzIPN.** Emission of a drop cast neat film of **4CzIPN** from toluene before and after annealing. The blue shift arises due to reduction in the dimer contribution with increased temperature. The temperature was raised to 250 °C for the annealing process. The dimer emission from the 532 nm excitation is shown for comparison.

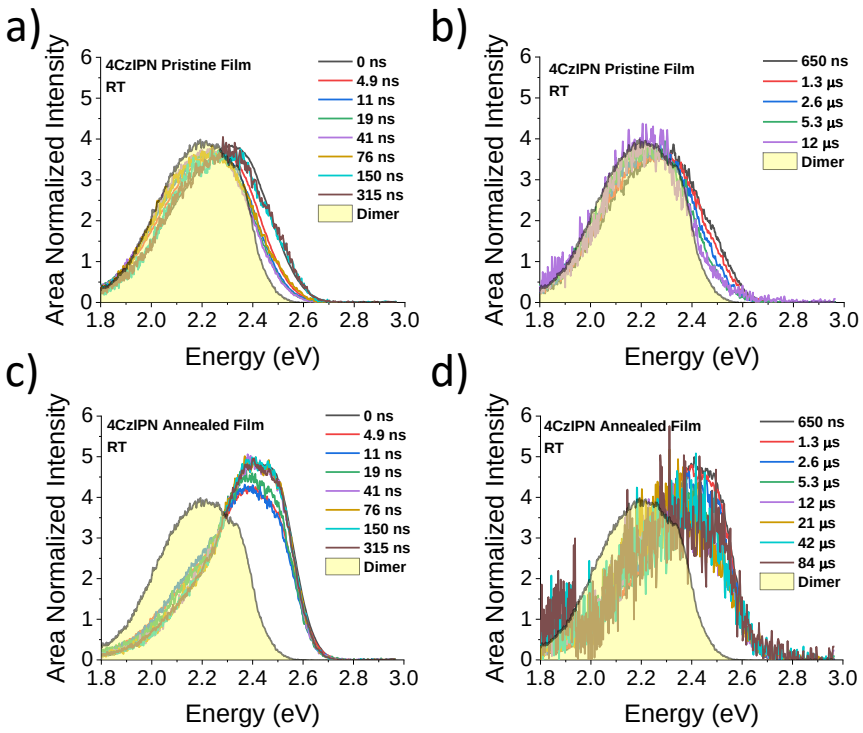

Figure S20 The time-resolved spectra of neat films of **4CzIPN** before and after annealing at RT. (**a-b**) The time resolved emission of the pristine neat film which is dominated by ^1CT_D emission apart from a small contribution from ^1CT_M of onset 2.7 eV. (**c-d**) The time resolved emission spectra of the same film after annealing. Both the prompt and delayed emission is significantly blue shifted due to the increase in ^1CT_M contribution. There is still a small contribution from ^1CT_D in the prompt, indicated by the shoulder at 2.2 eV.

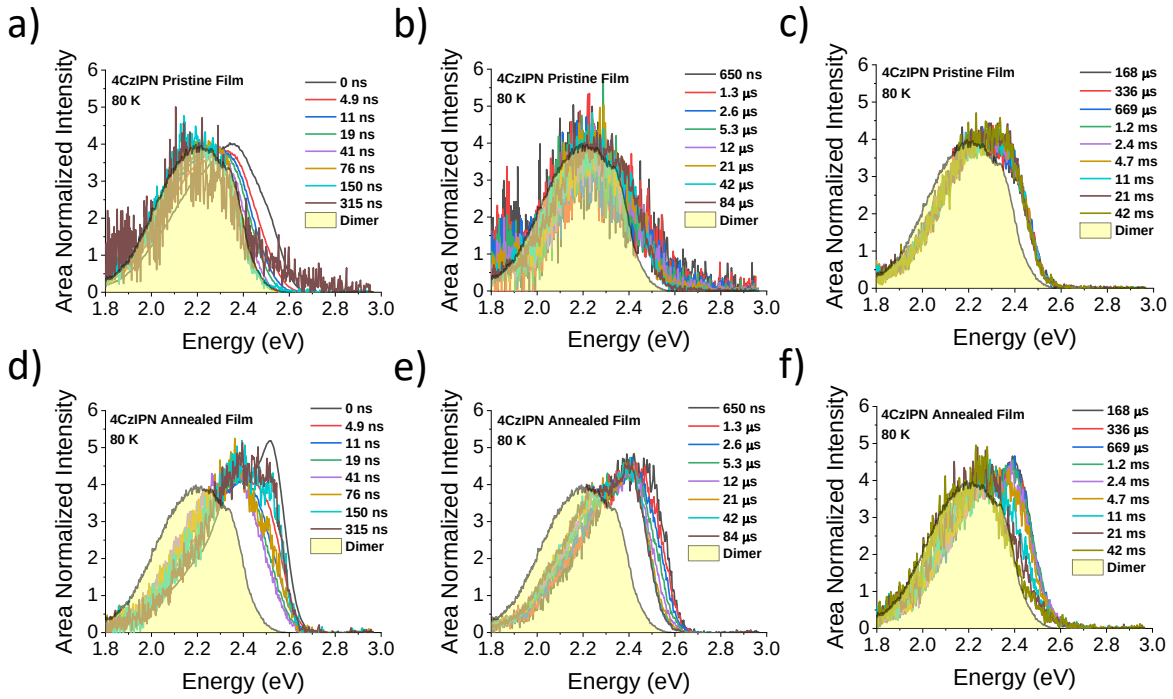

Figure S21 The time-resolved spectra of neat films of **4CzIPN** before and after annealing at 80 K. (**a-c**) The time-resolved emission of the pristine film at 80 K is dominated by the dimer emission. The long times are dominated by the phosphorescence of the ^3LE_D which has onset at 2.55 eV. (**d-f**) The annealed films spectra are dominated by the CT_M emission of onset 2.7eV, which is very close in energy to the monomer ^3LE at 2.7 eV. This explains the quite efficient TADF even at 80 K. At very long times the phosphorescence is dominated by the dimer phosphorescence, which is a consequence of the annealing process not destroying all dimer formation.

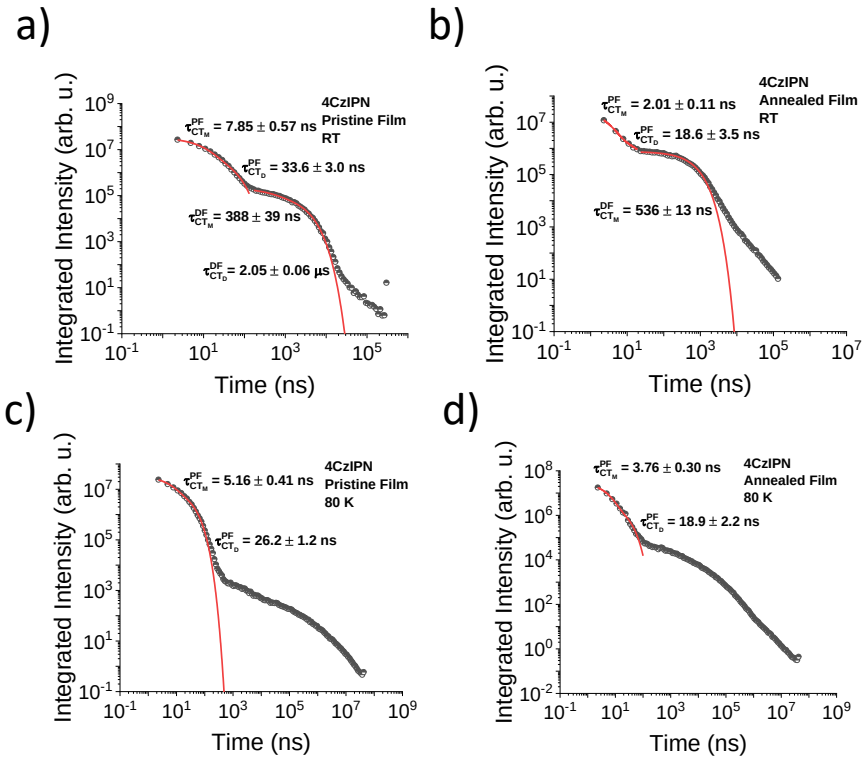

Figure S22 The time resolved photoluminescence decays of pristine and annealed **4CzIPN** neat films at RT and 80 K (**a**) **4CzIPN** pristine film and (**b**) annealed **4CzIPN** neat film at RT. (**c**) **4CzIPN** pristine film and (**d**) annealed **4CzIPN** neat film at 80 K. The decay fit parameters are shown in Tables S7 and S8.

11. PL spectroscopy of sublimed crystals of 4CzIPN

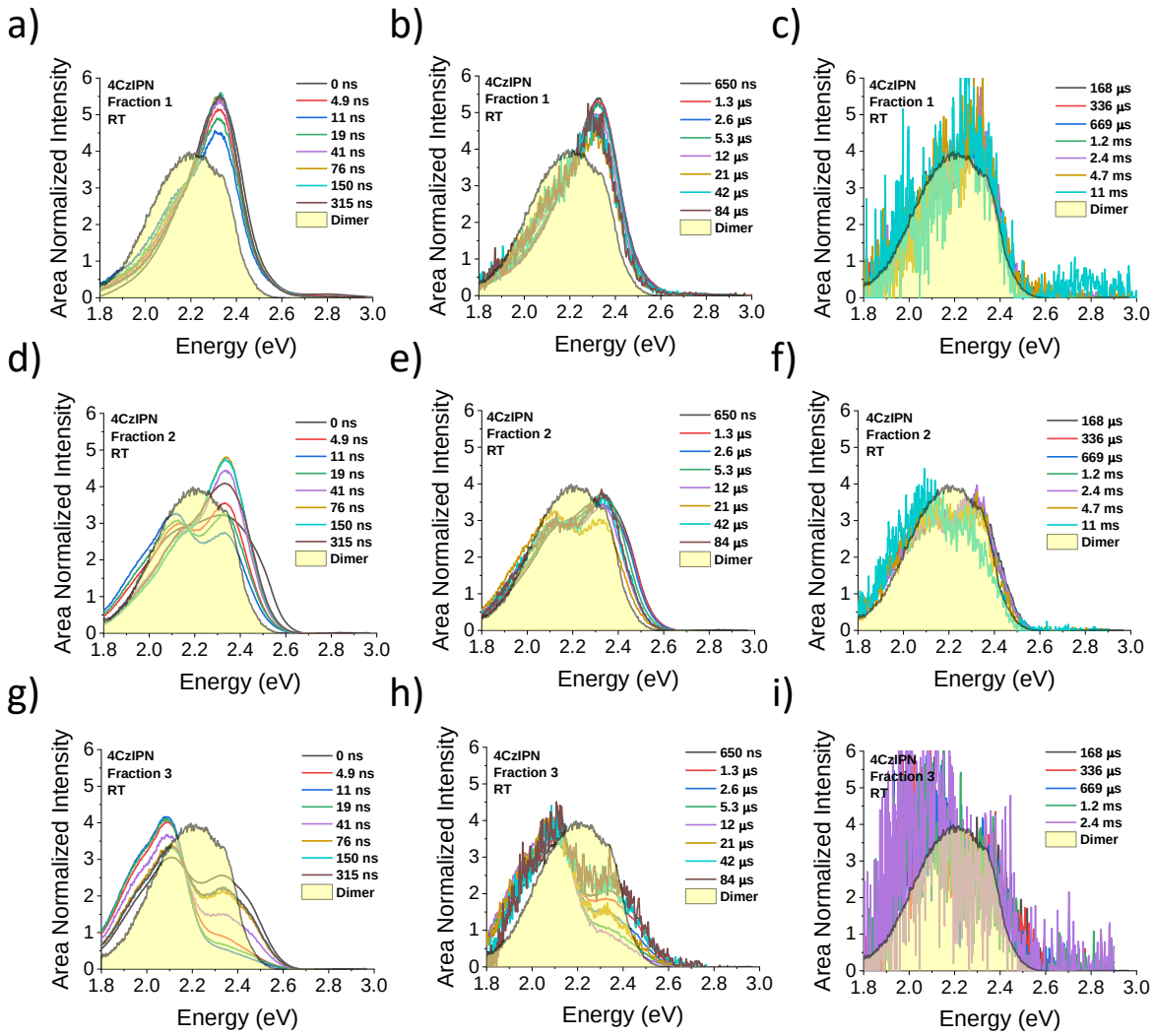

Figure S23 Time resolved spectra of **4CzIPN** sublimated fractions. (**a-c**) RT spectra of Fraction 1 **4CzIPN**. (**d-f**) RT spectra of Fraction 2 **4CzIPN**. (**g-i**) RT spectra of Fraction 3 **4CzIPN**.

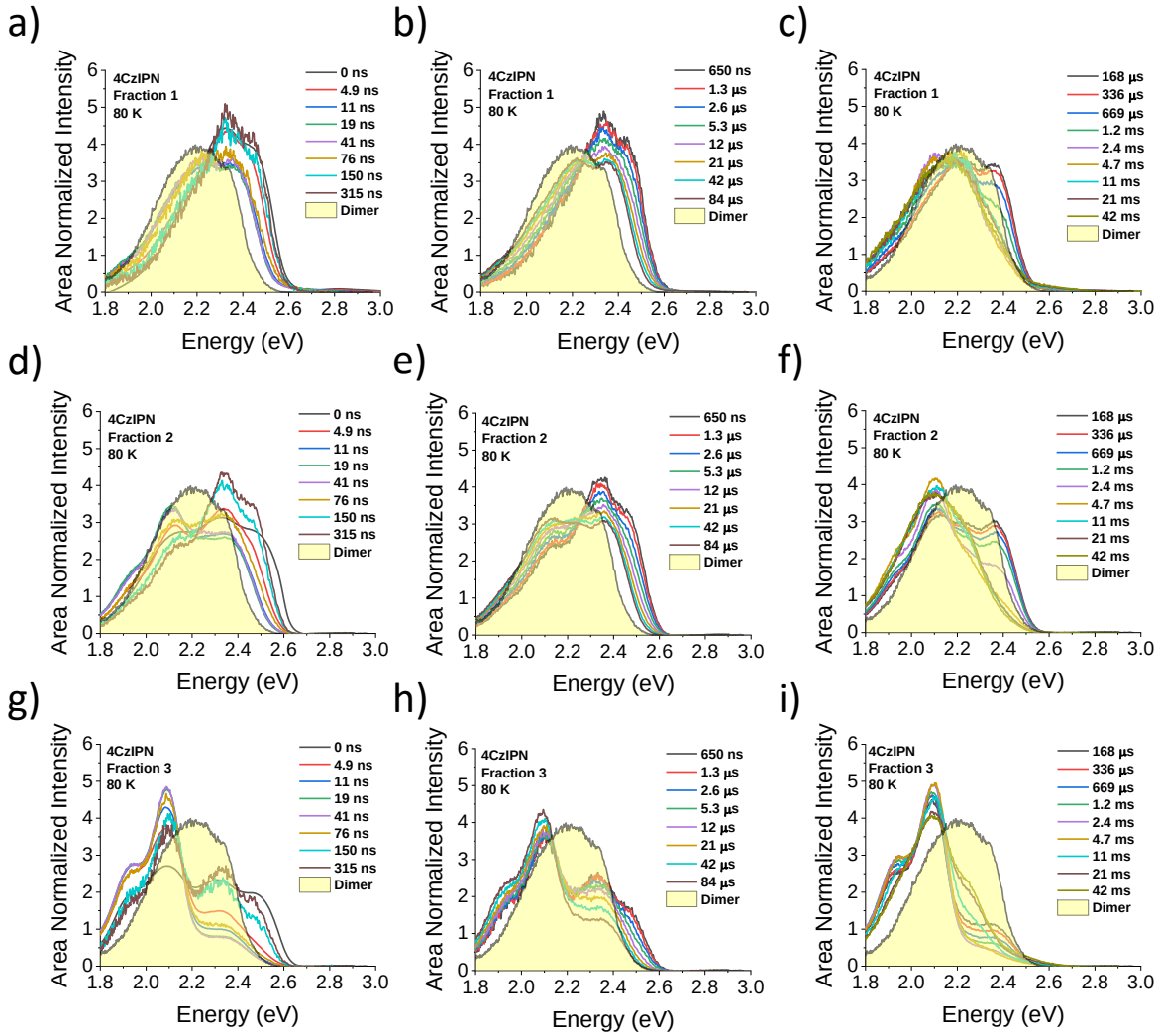

Figure S24 Time resolved spectra of **4CzIPN** sublimated fractions. (**a-c**) 80 K spectra of Fraction 1 **4CzIPN**. (**d-f**) 80 K spectra of Fraction 2 **4CzIPN**. (**g-i**) 80 K spectra of Fraction 3 **4CzIPN**.

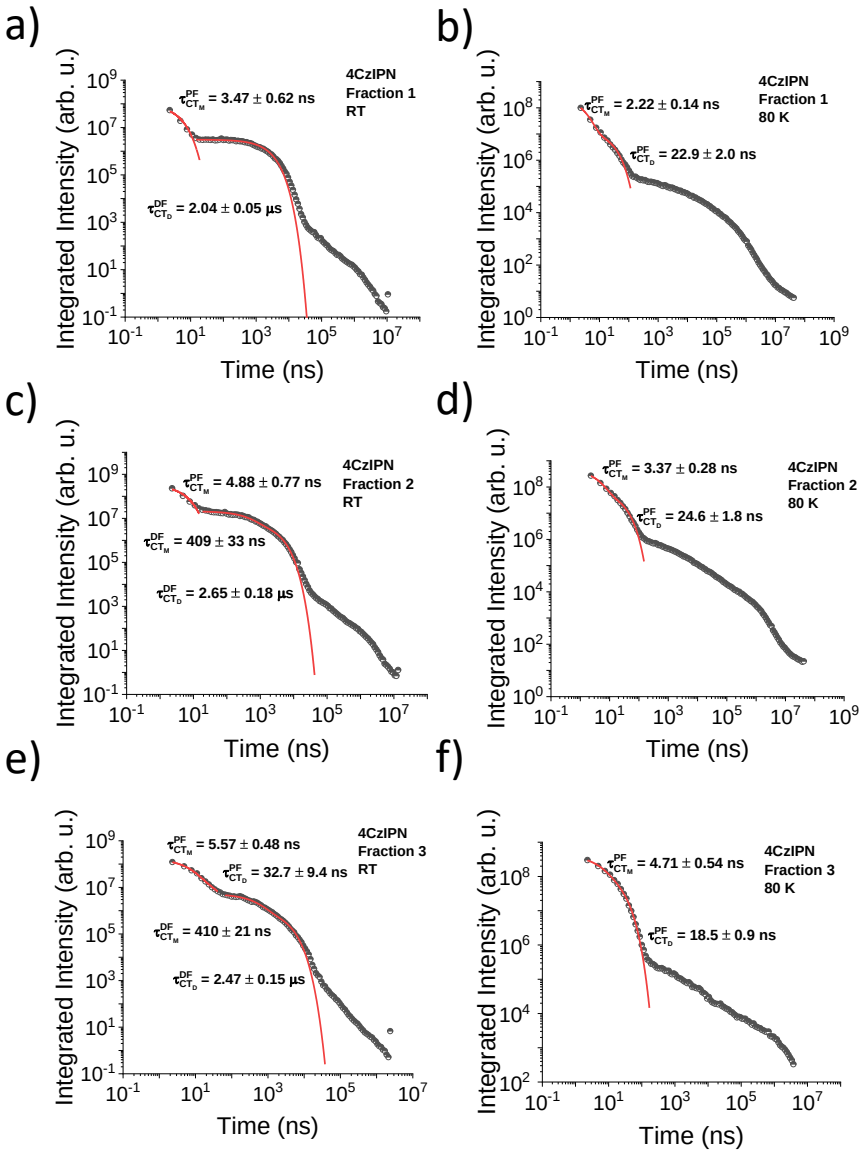

Figure S25 Photoluminescence decays of **4CzIPN** sublimed fractions. The photoluminescence decay of: Fraction 1 **4CzIPN** at (**a**) RT and (**b**) 80 K; Fraction 2 at (**c**) RT and (**d**) 80 K; and Fraction 3 at (**e**) RT and (**f**) 80 K. The decay fit parameters are found in Tables S9-11.

Table S9 The fitting parameters for the photoluminescence decays of Fraction 1 **4CzIPN** crystals grown from sublimation. The R^2 values for the fits are 0.87421 and 0.99256 for the PF and DF RT fits, and 0.99049 for the 80 K fit.

Temperature	aPF/CT(M)	τPF/CT(M)	aPF/CT(D)	τPF/CT(D)	aDF/CT(D)	τDF/CT(D)
RT	9.45E7 ± 2.41E7	3.47 ± 0.62	-	-	3.08E6 ± 0.04E6	2.04E3 ± 0.05E3
80 K	2.46E8 ± 0.20E8	2.22 ± 0.14	1.26E7 ± 0.15E7	22.9 ± 2.0	-	-

Table S10 The fitting parameters for the photoluminescence decays of the Fraction 2 **4CzIPN** crystals grown from sublimation. The R^2 values for the fits are 0.91267 and 0.99387 for the PF and DF RT fits, and 0.99983 for the 80 K fit.

Temperature	aPF/CT(M)	τPF/CT(M)	aPF/CT(D)	τPF/CT(D)	aDF/CT(M)	τDF/CT(M)	aDF/CT(D)	τDF/CT(D)
RT	3.34E8 ± 0.62E8	4.88 ± 0.77	-	-	1.46E7 ± 0.06E7	409 ± 33	6.29E6 ± 0.59E6	2.65E3 ± 0.18E3
80 K	4.11E8 ± 0.30E8	3.37 ± 0.28	6.27E7 ± 0.71E7	24.6 ± 1.8	-	-	-	-

Table S11 The fitting parameters for the photoluminescence decays of the Fraction 3 **4CzIPN** grown from sublimation. The R^2 values for the fits are 0.99754 and 0.99636 for the PF and DF RT fits, and 0.99689 for the 80 K fit.

Temperature	aPF/CT(M)	τPF/CT(M)	aPF/CT(D)	τPF/CT(D)	aDF/CT(M)	τDF/CT(M)	aDF/CT(D)	τDF/CT(D)
RT	1.50E8 ± 0.06E8	5.57 ± 0.48	2.29E7 ± 0.71E7	32.7 ± 9.4	4.19E6 ± 0.10E6	410 ± 21	1.07E6 ± 0.10E6	2.47E3 ± 0.15E3
80 K	2.73E8 ± 0.17E8	4.71 ± 0.54	1.45E8 ± 0.16E8	18.5 ± 0.9	-	-	-	-

12. Powder X-ray diffraction

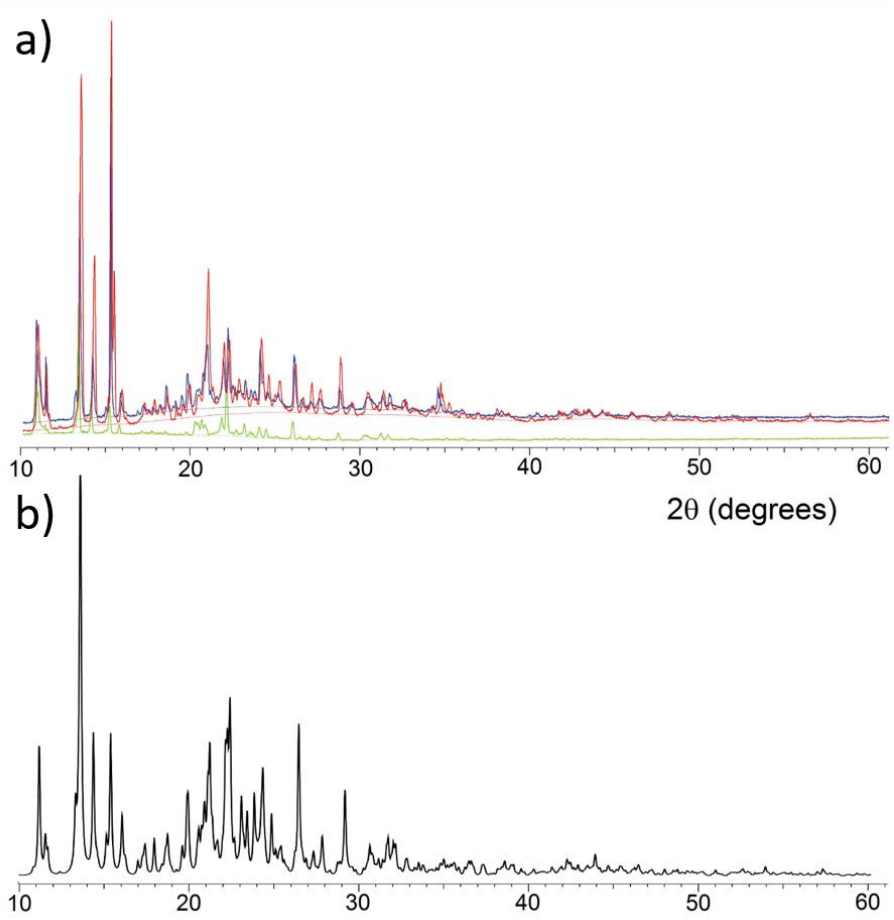

Figure S26 (a) Powder X-ray diffraction curves of sublimed **4CzIPN**, fractions **1** (red), **2** (blue) and **3** (green). (b) Simulated powder X-ray diffraction curve from single-crystal data of fraction **1**.

13. PL spectroscopy of solvent-grown crystals of 4CzIPN

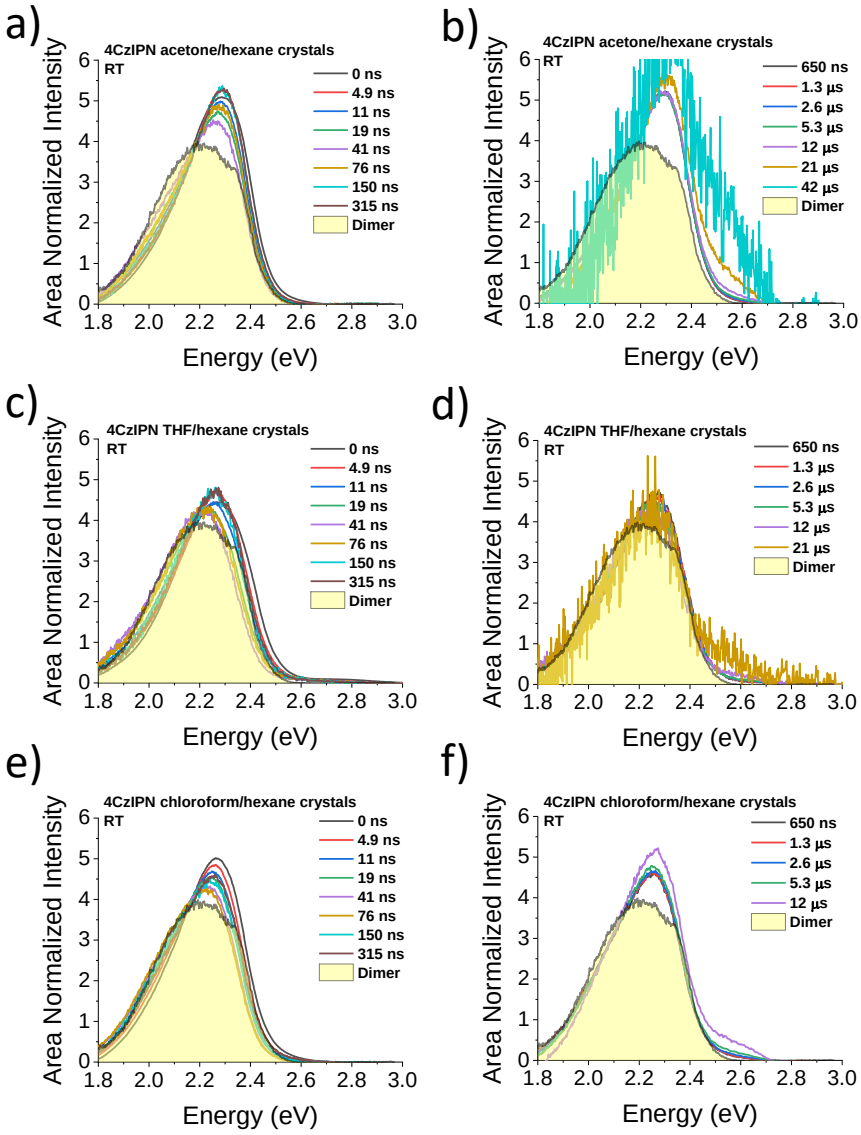

Figure S27 The time-resolved spectra of **4CzIPN** crystals grown from different solvents. (**a-b**) RT temperature spectra of **4CzIPN** crystals grown from acetone/hexanes. (**c-d**) RT spectra of **4CzIPN** crystals grown from THF/hexanes. (**e-f**) RT spectra of **4CzIPN** crystals grown from chloroform/hexanes.

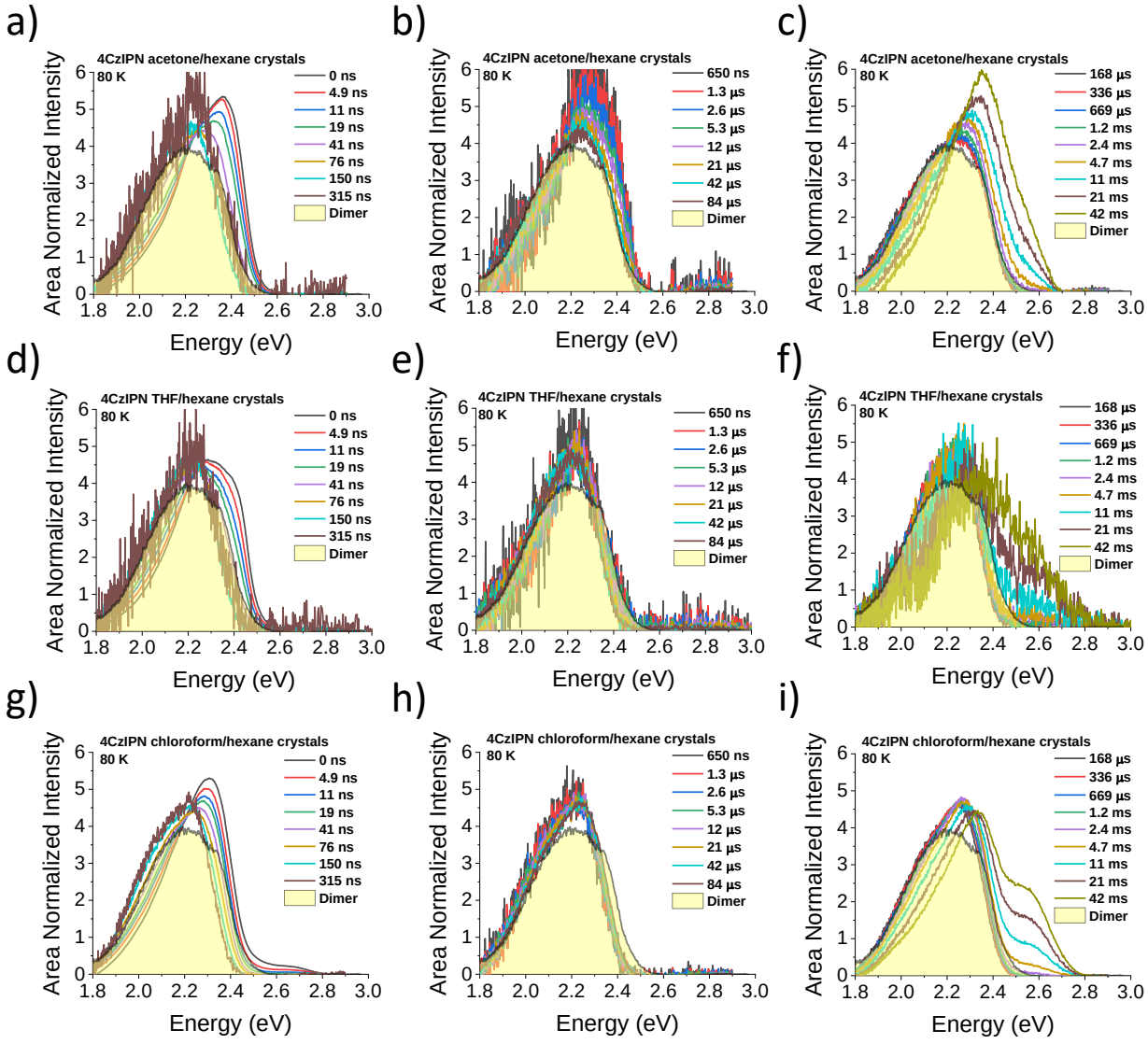

Figure S28 The time resolved spectra of **4CzIPN** crystals grown from different solvents. (**a-c**) 80 K spectra of **4CzIPN** crystals grown from acetone/hexanes. (**d-f**) 80 K spectra of **4CzIPN** crystals grown from THF/hexanes. (**g-i**) 80 K spectra of **4CzIPN** crystals grown from chloroform/hexanes.

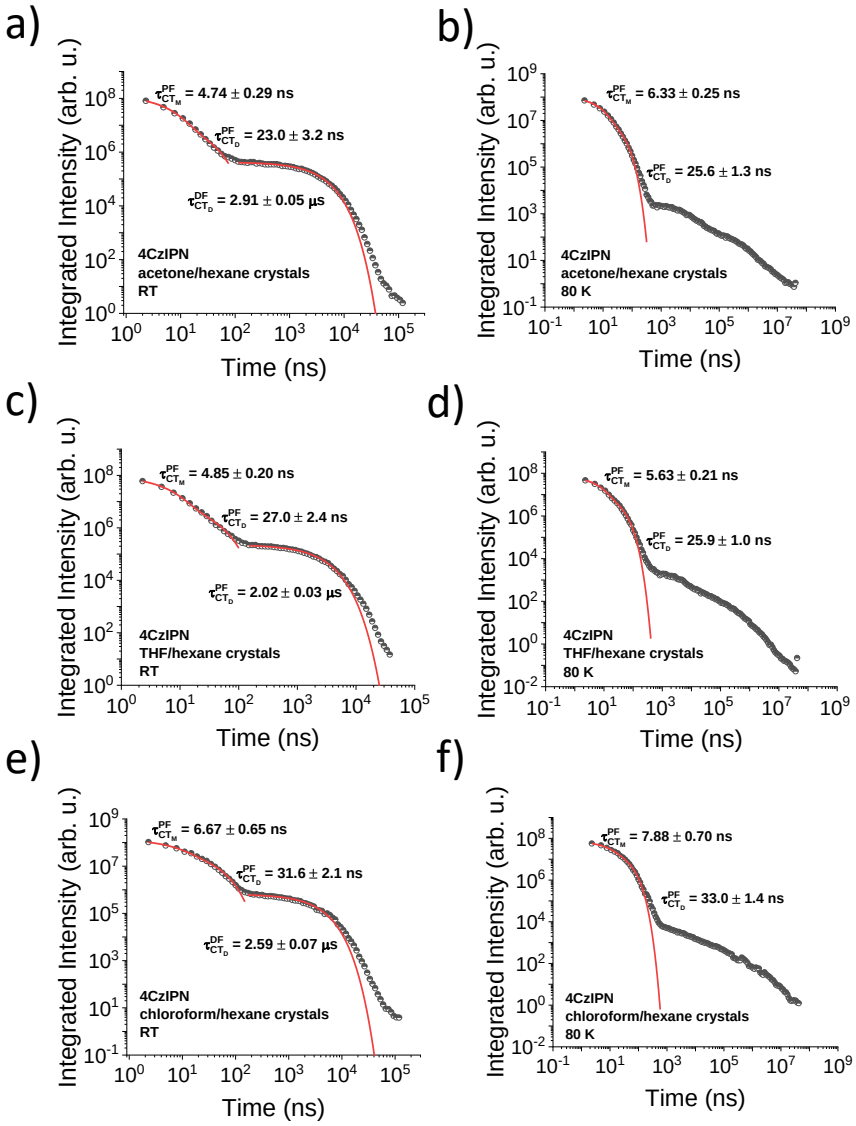

Figure S29 The photoluminescence decays of **4CzIPN** crystals grown from solvents. (**a**) RT decay and (**b**) 80 K decay of the acetone/hexanes crystals. (**c**) RT decay and (**d**) 80 K decay of the THF/hexanes crystals. (**e**) RT decay and (**f**) 80 K decay of the chloroform/hexanes crystals. The parameters of the fits for the decays are shown in Tables S12-14.

Table S12 The fitting parameters for the photoluminescence decays of the **4CzIPN** crystals grown from acetone/hexanes**.** The R^2 values for the fits are 0.99572 and 0.99645 for the PF and DF RT fits, and 0.99764 for the 80 K fit respectively.

Temperature	aPF/CT(M)	τPF/CT(M)	aPF/CT(D)	τPF/CT(D)	aDF/CT(D)	τDF/CT(D)
RT	1.14E8 ± 0.05E8	4.74 ± 0.29	1.00E7 ± 0.25E7	23.0 ± 3.2	4.20E5 ± 0.04E5	2.91E3 ± 0.05E3
80 K	8.20E7 ± 0.19E7	6.33 ± 0.25	1.39E7 ± 0.15E7	25.6 ± 1.3	-	-

Table S13 The fitting parameters for the photoluminescence decays of the **4CzIPN** crystals grown from THF/hexanes. The R^2 values for the fits are 0.99711 and 0.99667 for the PF and DF RT fits, and 0.99829 for the 80 K fit.

Temperature	aPF/CT(M)	τPF/CT(M)	aPF/CT(D)	τPF/CT(D)	aDF/CT(D)	τDF/CT(D)
RT	8.56E7 ± 0.26E7	4.85 ± 0.20	6.90E6 ± 1.05E6	27.0± 2.4	2.25E5 ± 0.03E5	2.02E3 ± 0.03E3
80 K	5.53E7 ± 0.12E7	5.63 ± 0.21	1.04E7 ± 0.08E7	25.9 ± 1.0	-	-

Table S14 The fitting parameters for the photoluminescence decays of the **4CzIPN** crystals grown from chloroform/hexanes. The R^2 values for the fits are 0.99538 and 0.98974 for the PF and DF RT fits, and 0.99691 for the 80 K fit.

Temperature	aPF/CT(M)	τPF/CT(M)	aPF/CT(D)	τPF/CT(D)	aDF/CT(D)	τDF/CT(D)
RT	9.86E7 ± 0.53E7	6.67 ± 0.65	3.48E7 ± 0.43E7	31.6 ± 2.1	6.41E5 ± 0.12E5	2.59E3 ± 0.07E3
80 K	4.47E7 ± 0.22E7	7.88 ± 0.70	2.46E7 ± 0.21E7	33.0 ± 1.4	-	-

14. Molecular packing and interactions in the solids

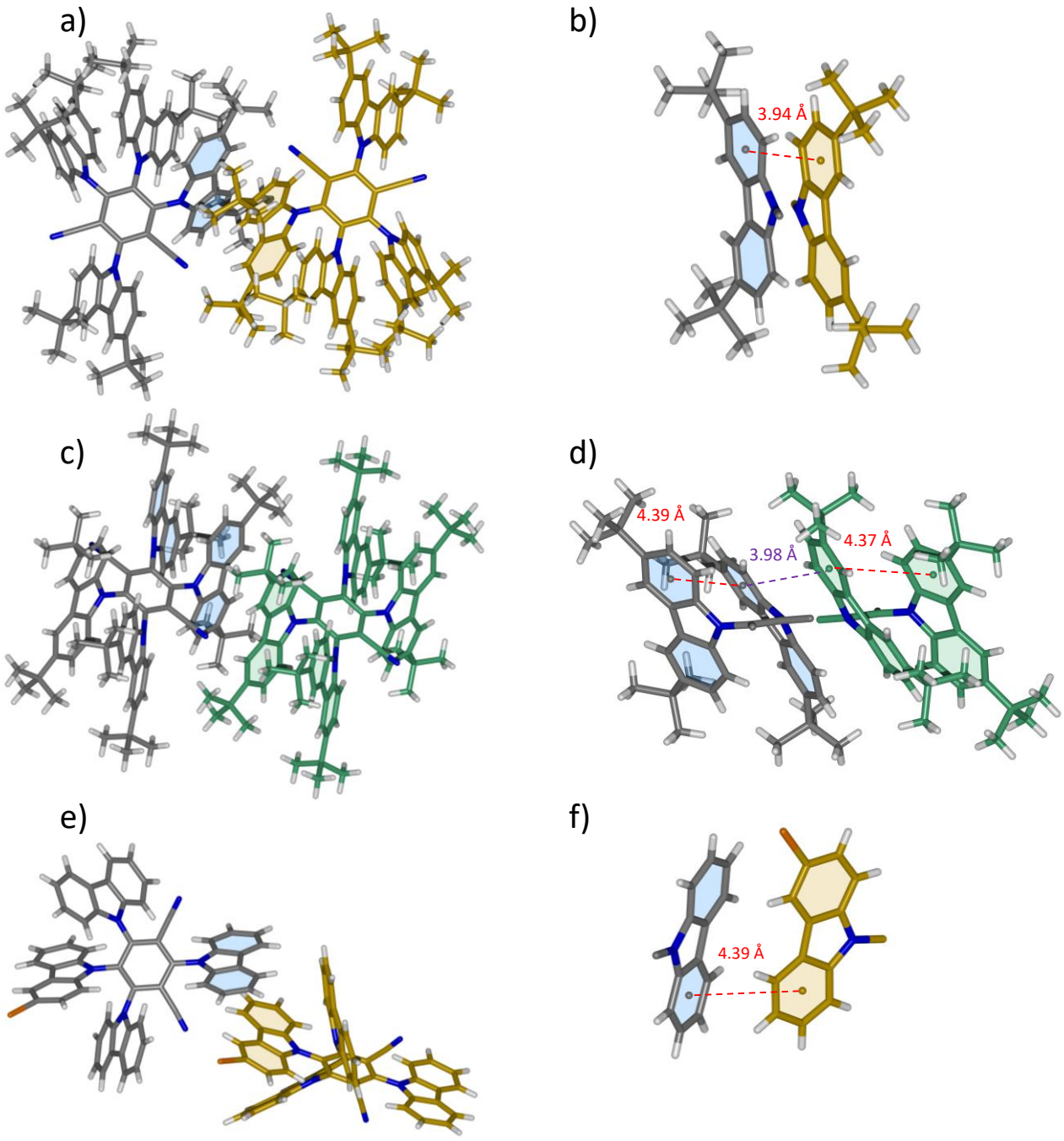

Figure S30 The crystal structures of **4CzIPN-^{t}Bu$_8$, 4CzTPN-^{t}Bu$_8$** and **4CzIPN-Br$_1$.** (**a**) **4CzIPN-^{t}Bu$_8$** packing behaviour and (**b**) the shortest distance between the interacting molecules. (**c**) The packing behaviour of **4CzTPN-^{t}Bu$_8$** and (**d**) the shortest distance between the interacting molecules. (**e**) The packing behaviour of **4CzIPN-Br$_1$** and (**f**) the shortest distance between the interacting molecules.

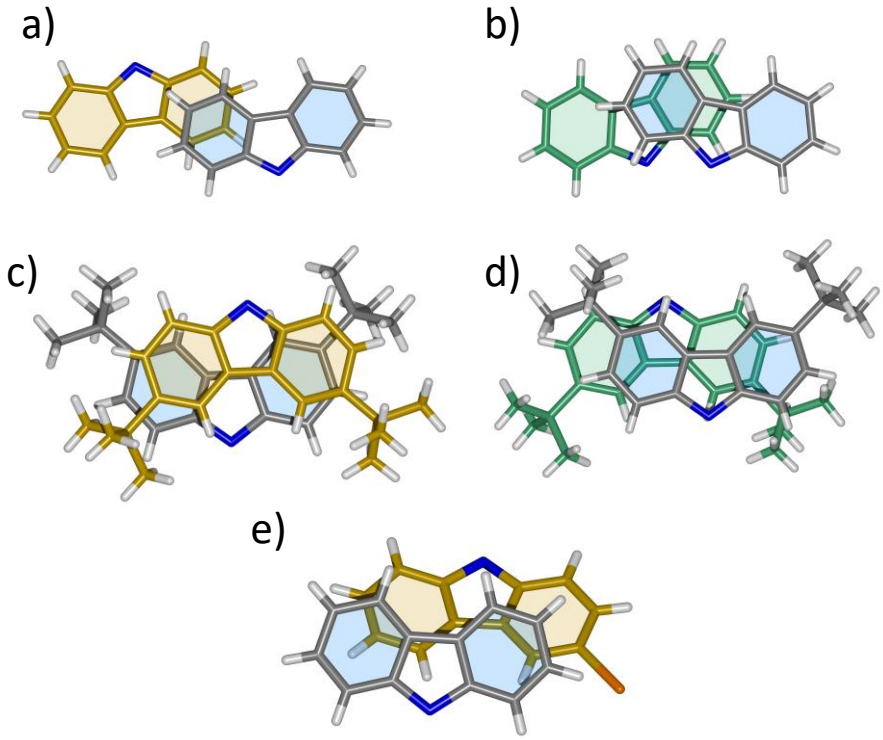

Figure S31 Overlap between the carbazoles from the crystal structures of the molecules. (**a**) **4CzIPN**, (**b**) **4CzTPN**, (**c**) **4CzIPN-^{t}Bu$_8$**, (**d**) **4CzTPN-^{t}Bu$_8$** and (**e**) **4CzIPN-Br$_1$**.

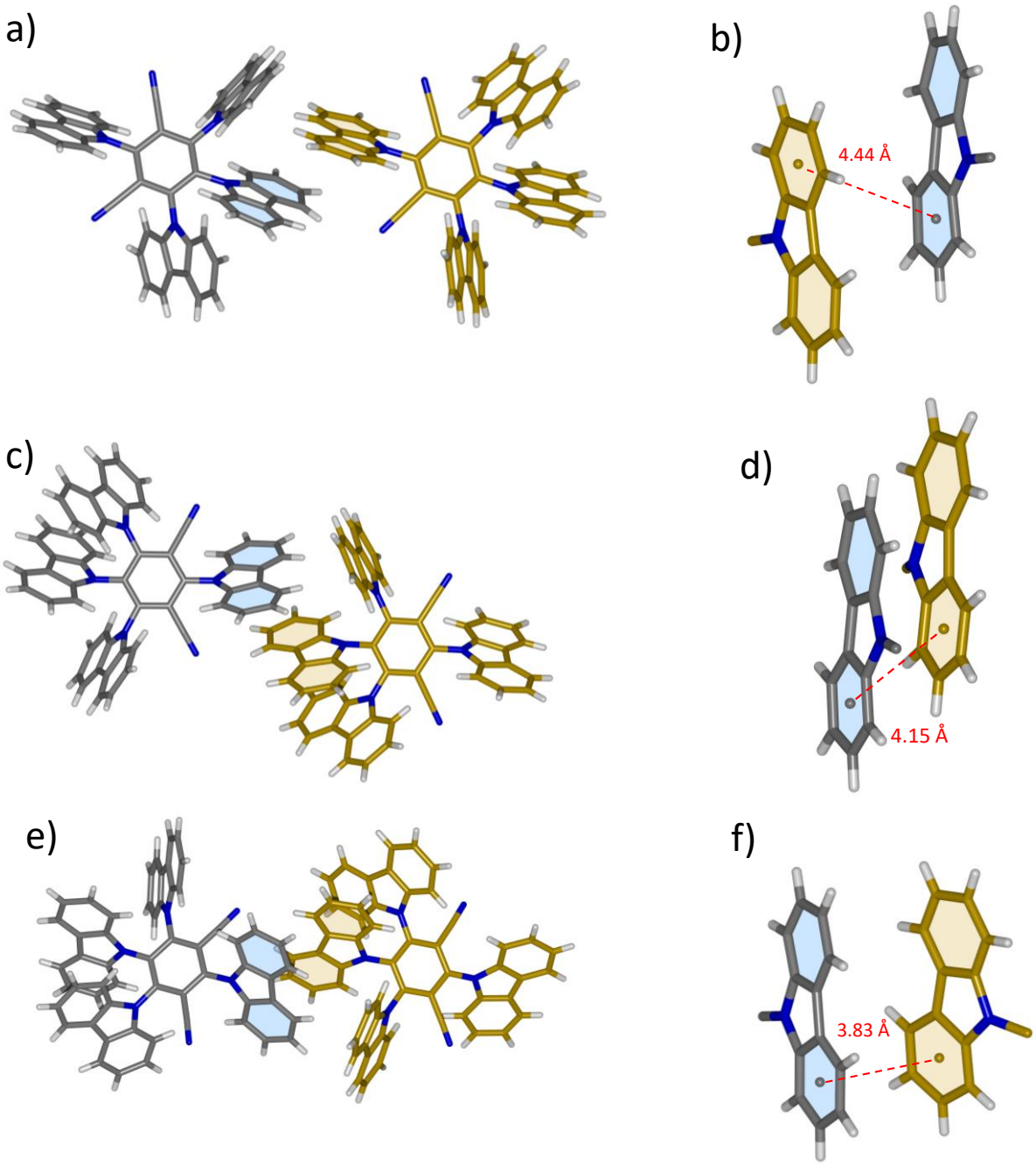

Figure S32 The crystal structures of **4CzIPN** grown from a variety of different solvents. (**a**) The packing behaviour and (**b**) closest distance between interacting molecules in acetone/hexanes grown crystal (**c**) The packing behaviour and (**d**) closest distance between interacting molecules in THF/hexanes grown crystal (**e**) The packing behaviour and (**f**) closest distance between interacting molecules in chloroform/hexanes grown crystal.

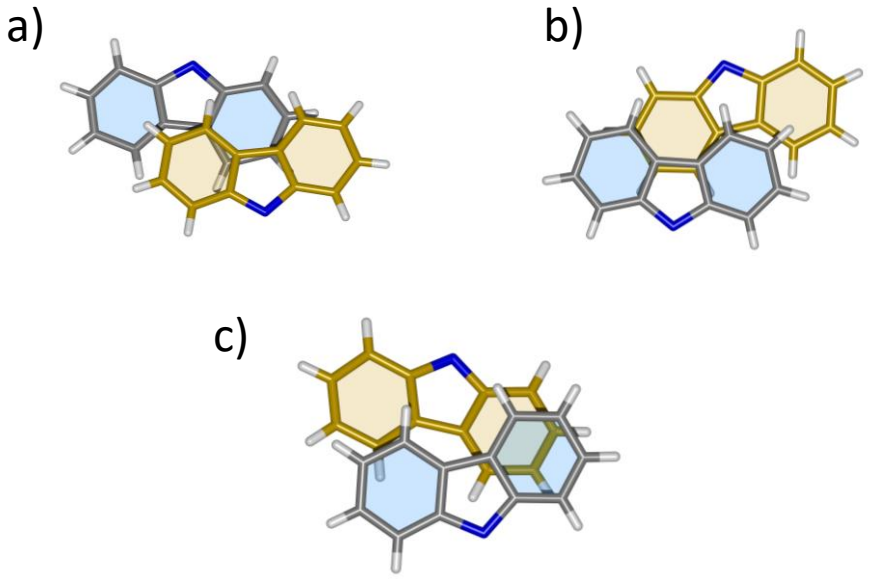

Figure S33 Overlap of the carbazoles for **4CzIPN** crystals grown from different solvents, (**a**) acetone/hexanes (**b**) THF/hexanes (**c**) chloroform/hexanes.

15. Differential scanning calorimetry and thermogravimetric analysis

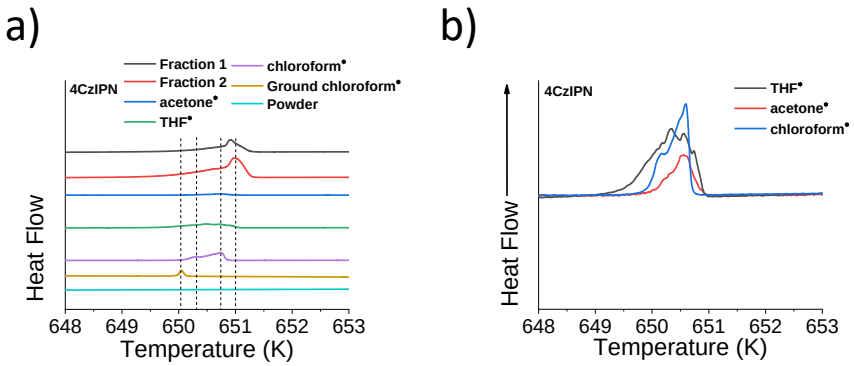

Figure S34 Differential scanning calorimetry curves of **4CzIPN** in different forms. DSC curves of (**a**) a collection of sublimated, solvent-grown, ground crystals and powder and (**b**) a high-resolution view of the three solvent grown crystals, collected under nitrogen atmosphere at a rate of 1 K/min. The different endothermic peaks represent the different melting points of the polymorphs in the **4CzIPN** molecule. The crystals grown from solvents with asterisks are a co-solvent of that and hexanes (i.e. the same crystals as demonstrated in the photophysical and crystallography data).

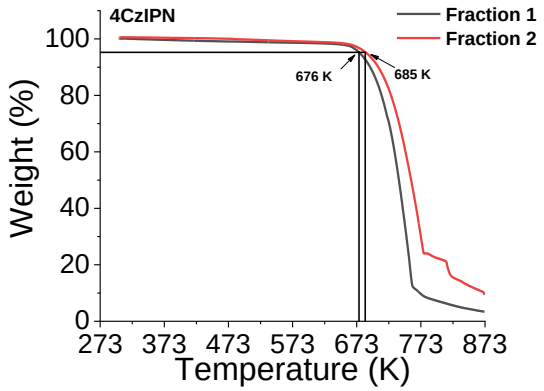

Figure S35 TGA curves of two of the sublimed fractions of **4CzIPN.**

16. PL spectroscopy of sublimed crystals of 4CzTPN

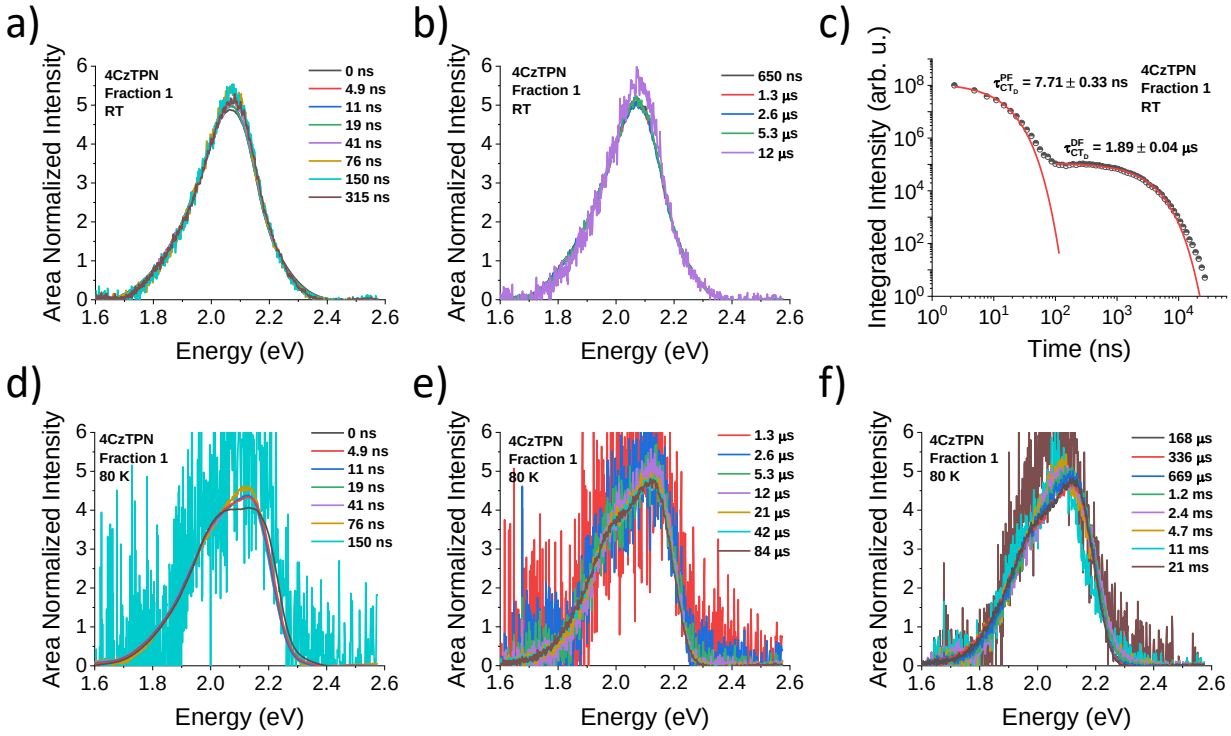

Figure S36 Time-resolved spectra of **4CzTPN** sublimated Fraction 1. The time-resolved photoluminescence spectra of sublimated **4CzTPN** (Fraction 1) at (**a-b**) RT and (**c**) the associated decay profile. The time-resolved photoluminescence of **4CzTPN** (Fraction 1) at (**d-f**) 80 K. Both at RT and 80 K there is no significant shift in the emission spectra over the emission time range.

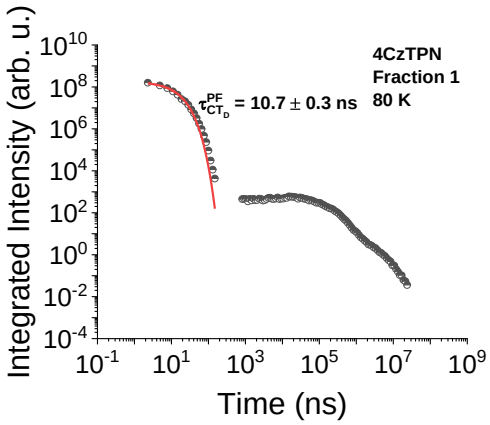

Figure S37 The time-resolved photoluminescence decays of **4CzTPN** (Fraction 1) at 80 K. The decay fit parameters are found in Table S15.

Table S15 The fitting parameters for the photoluminescence decays of **4CzTPN** crystals grown from sublimation. The R^2 values for the fits are 0.98345 and 0.99507 for the PF and DF RT fits, and 0.99082 for the 80 K fit respectively.

Temperature	aPF/CT(D)	τPF/CT(D)	aDF/CT(D)	τDF/CT(D)
RT	1.22E8 ± 0.06E8	7.71 ± 0.33	1.12E5 ± 0.01E5	1.89E3 ± 0.04E3
80 K	1.83E8 ± 0.06E8	10.7 ± 0.3	-	-

17. Mechanochromic luminescence

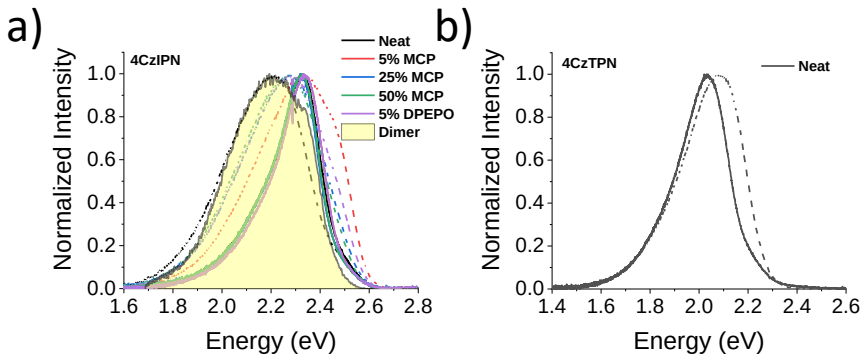

Figure S38 Mechanochromic luminescence of **4CzIPN** and **4CzTPN.** (**a**) The emission of **4CzIPN** as a neat crystal before grinding (solid lines) and after grinding (dashed lines) in a pestle and mortar either on its own (neat) or combined with powders of MCP and DPEPO, respectively. The percentage refers to the amount of **4CzIPN** in the host. (**b**) The emission of **4CzTPN** as a neat crystal before grinding (solid line) and after grinding (dashed line).

18. X-ray crystallography

X-ray diffraction experiments (Tables S16 and S17) were carried out on a Bruker 3-circle D8 Venture diffractometer with a PHOTON 100 CMOS area detector, using Mo-K_α or Cu-K_α radiation from Incoatec IμS microsources with focussing mirrors. Crystals were cooled using a Cryostream (Oxford Cryosystems) open-flow N_2 gas cryostat. The data were processed using APEX3 v.2016.1-0 and reflection intensities integrated using SAINT v8.38A software (Bruker AXS, 2016). **4CzIPN-^{t}Bu$_8$·C$_6$H$_{14}$** was studied at Beamline I19 of Diamond Light Source (RAL) on a dual air-bearing fixed-χ diffractometer with pixel-array photon-counting Dectris Pilatus 2M detector,[4] using undulator radiation monochromated with double-crystal Si(111). The crystal was cryo-mounted using remote-controlled BART robot[5] and cooled using a Cryostream N_2 gas cryostat. The diffraction images were converted to Bruker format using cbf_to_sfrm.py program[6] and further processed with APEX3 and SAINT software (*vide supra*).

Crystals of **4CzIPN**, **4CzIPN-^{t}Bu$_8$·C$_6$H$_{14}$** and **4CzIPN-^{t}Bu$_8$·2C$_6$H$_{14}$** crystallized as 2-component non-merohedral twins; the data were deconvoluted using CELL_NOW 2008/4 program and scaled using TWINABS 2012/1 program (Bruker AXS, 2008-2012). For other compounds, the data were corrected for absorption by semi-empirical method based on Laue equivalents and multiple scans (for **4CzIPN-Br$_1$** by numerical integration based on crystal face-indexing) using SADABS program.[7] The structures were solved by direct methods using SHELXS 2013/1 software[8] (**4CzIPN-Br$_1$** and **4CzIPN-^{t}Bu$_8$·C$_6$H$_{14}$** by dual-space intrinsic phasing method using SHELXT 2018/2 program[9]), and refined by full-matrix least squares using SHELXL 2018/3 software[10] on OLEX2 platform.[11]

Structures **4CzIPN-^{t}Bu$_8$·C$_6$H$_{14}$** and **4CzIPN-^{t}Bu$_8$·2C$_6$H$_{14}$** contain voids occupied by randomly disordered n-hexane which could not be refined at atomic resolution and was 'masked' (i.e. its contribution to the structure factors eliminated) using PLATON SQUEEZE program.[12] The asymmetric unit of **4CzIPN·1.8MeCN** contains two ordered and fully occupied MeCN molecules, three MeCN molecules with partial occupancies and one part-occupied MeCN molecule disordered around a twofold axis, which were refined, besides chaotically disordered solvent which was masked.

Table S16 Crystal data and experimental details

Compound	**4CzIPN**	**4CzIPN ·3THF**	**4CzIPN ·3.5Me_2CO**	**4CzIPN ·3$CHCl_3$**	**4CzIPN ·1.8MeCN**	**4CzIPN·0.8CH_2Cl_2 ·0.8Me_2CO·0.2C_6H_{14}**
Local depository no.	18srv040	18srv019	18srv437	18srv073	17srv336	18srv002
CCDC no.	1873416	1873417	1873418	1873419	1873420	1873421
Formula	$C_{56}H_{32}N_6$	$C_{68}H_{56}N_6O_3$	$C_{66.5}H_{53}N_6O_{3.5}$	$C_{59}H_{35}Cl_9N_6$	$C_{59.6}H_{37.4}N_{7.8}$	$C_{60.4}H_{41.2}Cl_{1.6}N_6O_{0.8}$
Formula Weight	788.87	1005.18	992.15	1146.98	862.43	920.51
Crystal System	triclinic	monoclinic	monoclinic	monoclinic	monoclinic	triclinic
Space Group	$P\bar{1}$ (# 2)	$P2_1/n$ (# 14)	$P2_1/n$ (# 14)	$P2_12_12_1$ (# 19)	$C2/c$ (# 15)	$P\bar{1}$ (# 2)
a/Å	8.9077(6)	13.2748(5)	13.5010(5	13.6522(10)	70.128(3)	13.0766(12)
b/Å	19.4451(13)	23.4797(9)	23.4890(9)	16.8556(12)	21.4702(8)	13.5258(13)
c/Å	23.7968(15)	17.4296(6)	17.2129(7)	22.942(2)	18.5758(7)	15.2752(13)
α/°	78.143(3)	90	90	90	90	80.949(4)
β/°	84.235(3)	100.334(2)	101.522(1)	90	94.086(2)	66.259(3)
γ/°	89.989(3)	90	90	90	90	71.062(4)
V/Å^3	4012.6(5)	5344.5(3)	5348.6(4)	5279.4(7)	27897.7(18)	2338.1(4)
$D_{calc.}$/ g cm^{-3}	1.306	1.249	1.232	1.443	1.232	1.307
μ/mm^{-1}	0.08	0.08	0.08	0.52	0.58	0.17
T/ K	120	120	120	120	120	120

Radiation	Mo-K_α	Mo-K_α	Mo-K_α	Mo-K_α	Cu-K_α	Mo-K_α
λ/Å	0.71073	0.71073	0.71073	0.71073	1.54184	0.71073
Z	4	4	4	4	24	2
$2\theta_{max}$/°	50	50	50	53	133.2	53.5
Measured reflections	53484	74436	73332	94722	105910	34292
Independent reflections	22678	9409	9415	10943	21174	9925
Reflections with $I>2\sigma(I)$	13563	7271	7366	9710	5799	7458
R_{int}	0.045	0.053	0.037	0.051	0.193	0.039
Parameters/restraints	1119/1116	704/36	811/86	679/10	1779/1545	666/21
Δρ/ eÅ^{-3} max/min	0.40, -0.38	0.53, -0.44	0.50, -0.37	0.64, -0.65	0.43,-0.28	0.56, -0.55
Goodness of fit	1.012	1.028	1.040	1.034	0.998	1.042
R_1 , wR_2 (all data)	0.147, 0.224	0.068, 0.123	0.076, 0.164	0.056, 0.124	0.213, 0.227	0.071, 0.132
R_1 , wR_2 , $I>2\sigma(I)$	0.079, 0.187	0.048, 0.111	0.058, 0.150	0.046, 0.118	0.083, 0.174	0.048, 0.122

Table S17 Crystal data and experimental details

Compound	**4CzIPN-Br_1 ·2 MeCN**	**4CzIPN-Br_1 ·2 MeCN**	**4CzIPN-^{t}Bu_8 ·$2C_6H_{14}$**	**4CzIPN-^{t}Bu_8 ·C_6H_{14}**	**4CzTPN**	**4CzTPN-^{t}Bu_8**
Local depository no.	18srv101	18srv127	18srv136	17srv321	18srv150	18srv168
CCDC no.	1873422	1873423	1873424	1873427	1873425	1873426
Formula	$C_{60}H_{37}BrN_8$	$C_{60}H_{37}BrN_8$	$C_{100}H_{120}N_6$	$C_{94}H_{110}N_6$	$C_{56}H_{32}N_6$	$C_{88}H_{96}N_6$
Formula Weight	949.88	949.88	1406.01	1323.87	788.87	1237.70
Crystal System	monoclinic	monoclinic	triclinic	triclinic	monoclinic	triclinic
Space Group	$P2_1/n$ (# 14)	$P2_1/n$ (# 14)	$P\bar{1}$ (# 2)	$P\bar{1}$ (# 2)	$P2_1/n$ (# 14)	$P\bar{1}$ (# 2)
a/Å	10.9331(3)	10.8305(9)	11.9194(4)	11.7820(5)	17.1156(10)	11.2959(5)
b/Å	19.6323(6)	19.5979(16)	18.1784(6)	17.9094(7)	10.1624(6)	11.6028(5)
c/Å	22.4761(6)	22.3531(18)	20.0895(7)	20.0156(8)	22.5700(13)	15.7669(7)
α/°	90	90	97.775(2)	98.415(2)	90	102.481(2)
β/°	102.340(2)	102.385(3)	99.395(2)	100.812(2)	93.262(2)	96.643(2)
γ/°	90	90	101.293(2)	102.134(2)	90	116.454(2)
V/Å^3	4712.9(2)	4634.1(7)	4148.0(2)	3979.2(3)	3919.4(4)	1752.48(14)
$D_{calc.}$/ g cm^{-3}	1.339	1.249	1.126	1.105	1.337	1.173
μ/mm^{-1}	1.58	0.94	0.58	0.06	0.08	0.07
T/ K	200	120	120	100	120	120

Radiation	Cu-K_α	Mo-K_α	Cu-K_α	synchrotron	Mo-K_α	Mo-K_α
λ/Å	1.54184	0.71073	1.54184	0.6889	0.71073	0.71073
Z	4	4	2	2	4	1
$2\theta_{max}$/°	138	50.3	149.6	58.35	55.1	53.5
Measured reflections	57821	56460	31736	75901	72476	31701
Independent reflections	8763	8235	14567	40673	9042	7439
Reflections with $I>2\sigma(I)$	6359	6841	7800	31568	6689	5280
R_{int}	0.076	0.064	0.050	0.039	0.071	0.047
Parameters/restraints	604/36	641/526	1779/1545	947/48	560/0	462/6
Δρ/ eÅ^{-3} max/min	0.39, -0.53	0.69, -0.83	0.27,-0.27	0.67, -0.32	0.27, -0.25	0.38, -0.37
Goodness of fit	1.117	1.281	1.047	1.113	1.030	1.022
R_1 , wR_2 (all data)	0.105, 0.200	0.099, 0.181	0.119, 0.199	0.095, 0.234	0.070, 0.107	0.081, 0.130
R_1 , wR_2 , $I>2\sigma(I)$	0.080, 0.187	0.082, 0.175	0.069, 0.169	0.080, 0.216	0.044, 0.096	0.051, 0.117

4CzIPN was studied as an unsolvated form identical with that reported earlier at room temperature (YUGDOV) and five different solvates ('pseudo-polymorphs'), viz. **4CzIPN·3THF**, **4CzIPN·3CHCl$_3$**, **4CzIPN·3.5Me$_2$CO**, **4CzIPN·1.8MeCN**, and a mixed DCM/acetone/hexanes solvate. The crystals of the THF and chloroform solvates are isomorphous. The asymmetric unit of unsolvated **4CzIPN** contains two independent molecules with practically identical conformation (Figure S40), whereby the planar carbazolyl (Cz) substituents *i, ii* and *iii* are inclined to the central benzene plane *iv* in a propeller-like fashion, while Cz-*v* is inclined in the opposite sense and is approximately related to Cz-*ii* by an inversion about the benzene ring centre, planes *ii* and *v* being eclipsed within 4º. All Cz/benzene interplanar angles (52-63º) are too wide for π-conjugation. The solvated forms have one independent **4CzIPN** molecule each, except the acetonitrile solvate which has three. All of them adopt broadly similar conformations with the Cz/benzene angles (54-75º) on average wider than in pure **4CzIPN**, except that in the 'mixed' solvate Cz-*v* is rotated in the *same* sense as the rest and staggered by 44.6º with respect to Cz-*ii*, hence the entire molecule has a roughly twofold axis passing through rings *ii*, *iv* and *v* (Figure S41). Mostly, carbazolyl N atoms are planar-trigonal, so that the extra-cyclic N-C bond is coplanar with the Cz plane. However, occasionally this bond is substantially tilted out of the Cz plane (Figure S42), most prominently for Cz-*ii* in the THF (21º tilt), chloroform (12º), acetone (10º) and 'mixed' solvate (10º), as well as for Cz-*i* in *two* independent **4CzIPN** molecules of the acetonitrile solvate (11º and 16º). The tilts usually facilitate intermolecular π-π stacking. Another recurrent mode of distortion is a librational disorder of a Cz group, which could be described by two alternative positions tilted to opposite sides of the benzene ring, with equal or near-equal probability. This is exhibited by Cz-*ii* in the acetone solvate (Figure S43, libration arch of 26º), and by a Cz-*i* (25º arch) and a Cz-*v* (16º arch) of two independent molecules in the acetonitrile solvate, the third molecule showing no disorder. Details of the Cz/benzene dihedral angles are shown in Table S18.

Table S18 Cz/benzene dihedral angles (º)

Compound	i/iv	ii/iv	iii/iv	v/iv
4CzIPN[a]	55.8	63.0	56.7	59.0
	52.3	63.2	57.4	59.5
4CzIPN·3THF	61.9	62.5	70.2	61.7
4CzIPN·3CHCl$_3$	63.6	60.6	62.2	53.8
4CzIPN·3.5Me$_2$CO	63.5	61.7[b]	70.0	65.8
4CzIPN·1.8MeCN[c]	58.8	67.9	67.1	58.4
	62.3	64.0	70.8	64.5,72.6[b]
	74.6[b]	66.1	62.1	61.3
4CzIPN·solv.	66.2	67.5	72.3	71.3

[a] Two independent molecules; [b]disordered Cz groups; [c]three independent molecules.

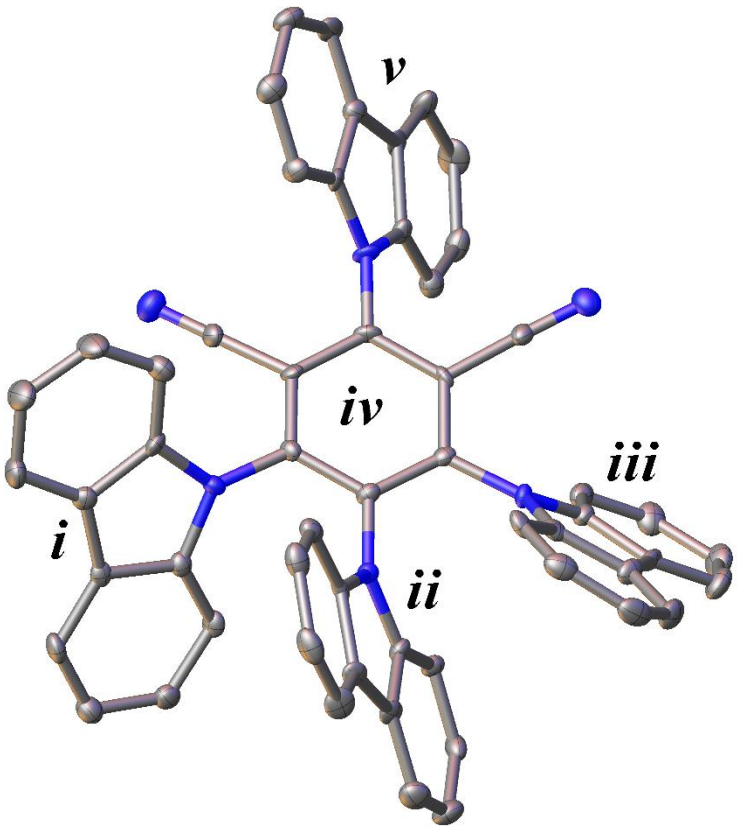

Figure S39 One of the independent molecules in the structure of sublimated **4CzIPN** at 120 K. It shows thermal ellipsoids at the 50% probability level and the notation of planar moieties. H atoms are omitted for clarity.

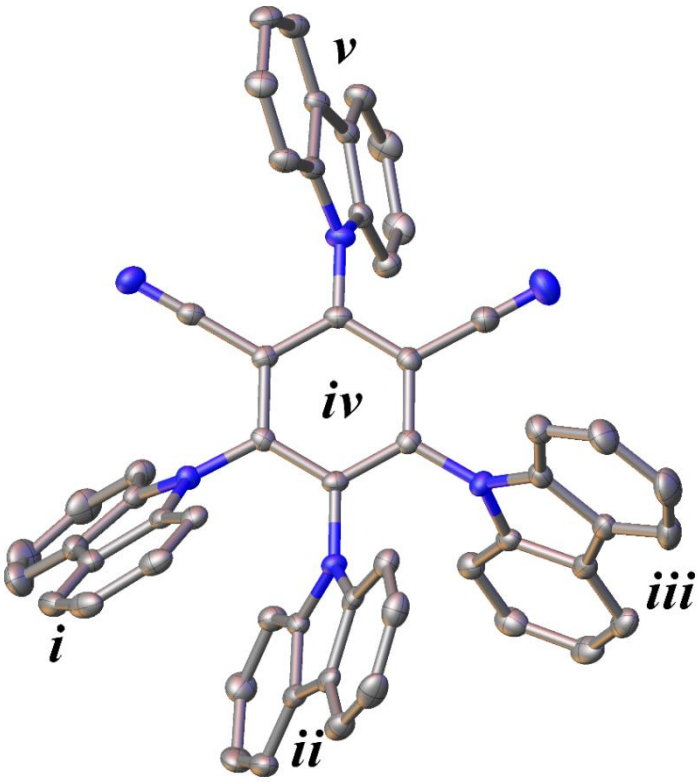

Figure S40 4CzIPN molecule in the DCM/acetone/hexanes solvate.

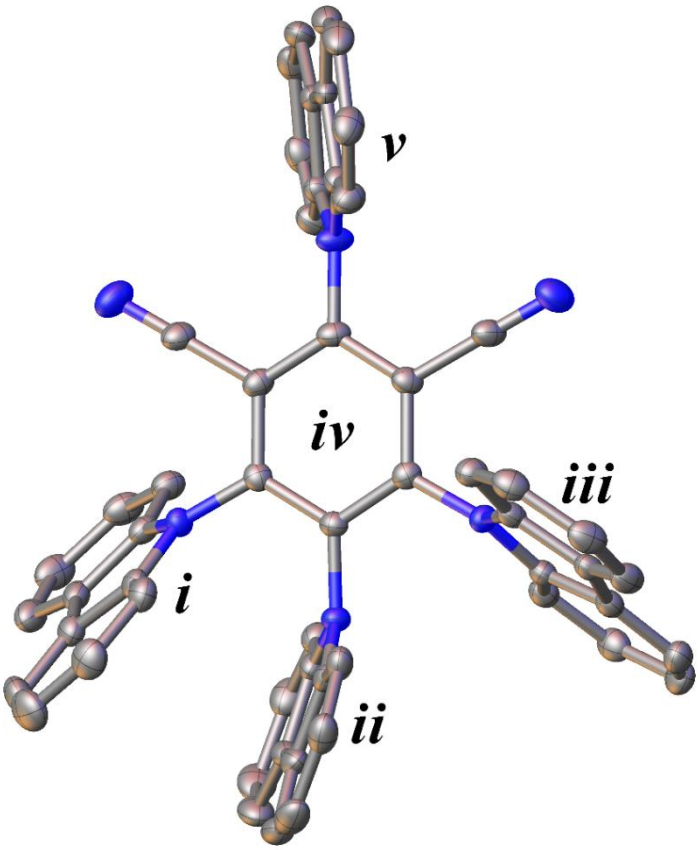

Figure S41 4CzIPN molecule in the THF solvate. Note the tilt of the carbazolyl moiety ii.

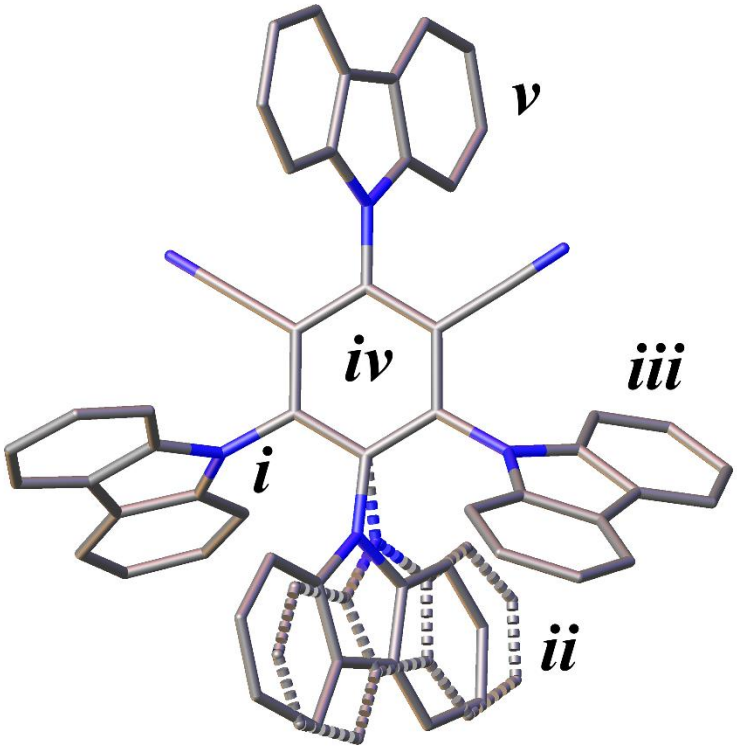

Figure S42 4CzIPN molecule in the acetone solvate. It shows librational disorder of the carbazolyl moiety *ii*.

19. References

1 C. Liu, R. Dai, G. Yao and Y. Deng, *J. Chem. Res.*, 2014, **38**, 593–596.

2 R. Ishimatsu, T. Edura, C. Adachi, K. Nakano and T. Imato, *Chem. - A Eur. J.*, 2016, **22**, 4889–4898.

3 F. A. Neugebauer and H. Fischer, *Chem. Ber.*, 1972, **105**, 2686–2693.

4 D. . Allan, H. Nowell, S. Barnett, M. Warren, A. Wilcox, J. Christensen, L. Saunders, A. Peach, M. Hooper, L. Zaja, S. Patel, L. Cahill, R. Marshall, S. Trimnell, A. Foster, T. Bates, S. Lay, M. Williams, P. Hathaway, G. Winter, M. Gerstel and R. Wooley, *Crystals*, 2017, **7**, 336.

5 N. Johnson, P. Waddell, W. Clegg and M. Probert, *Crystals*, 2017, **7**, 360.

6 N. T. Johnson and M. R. Probert, cbf_to_sfrm.py (α Version), https://github.com/nu-xtal-tools/cbf_to_sfrm.

7 L. Krause, R. Herbst-Irmer, G. M. Sheldrick and D. Stalke, *J. Appl. Crystallogr.*, 2015, **48**, 3–10.

8 G. M. Sheldrick, *Acta Crystallogr. Sect. A Found. Crystallogr.*, 2008, **64**, 112–122.

9 G. M. Sheldrick, *Acta Crystallogr. Sect. A Found. Crystallogr.*, 2015, **71**, 3–8.

10 G. M. Sheldrick, *Acta Crystallogr. Sect. C Struct. Chem.*, 2015, **71**, 3–8.

11 O. V. Dolomanov, L. J. Bourhis, R. J. Gildea, J. A. K. Howard and H. Puschmann, *J. Appl. Crystallogr.*, 2009, **42**, 339–341.

12 A. L. Spek, *Acta Crystallogr. Sect. C Struct. Chem.*, 2015, **71**, 9–18.